Inorganic Chemistry

Article

pubs.acs.org/IC

Indolenine *meso*-Substituted Dibenzotetraaza[14]annulene and Its Coordination Chemistry toward the Transition Metal Ions Mn^{III}, Fe^{III}, Co^{II}, Ni^{II}, Cu^{II}, and Pd^{II}

Hamid Khaledi,*[,†] Marilyn M. Olmstead,[‡] Hapipah Mohd Ali,[†] and Noel F. Thomas[†]

[†]Department of Chemistry, University of Malaya, Kuala Lumpur 50603, Malaysia

[‡]Department of Chemistry, University of California, Davis, California 95616, United States

Supporting Information

ABSTRACT: A new dibenzotetraaza[14]annulene bearing two 3,3-dimethylindolenine fragments at the *meso* positions (LH_2), has been synthesized through a nontemplate method. X-ray crystallography shows that the whole molecule is planar. The basicity of the indolenine ring permits the macrocycle to be protonated external to the core and form $LH_4^{2+}\cdot 2Cl^-$. Yet another structural modification having strong C−H···π interactions was found in the chloroform solvate of LH_2. The latter two modifications are accompanied by a degree of nonplanar distortion. The antiaromatic core of the macrocycle can accommodate a number of metal ions, Mn^{III}, Fe^{III}, Co^{II}, Ni^{II} and Cu^{II}, to form complexes of [Mn(**L**)Br], [Mn(**L**)Cl], $[Fe(LH_2)Cl_2]^+\cdot Cl^-$, [Co(**L**)], [Ni(**L**)], and [Cu(**L**)]. In addition, the reaction of LH_2 with the larger Pd^{II} ion leads to the formation of $[Pd_2(LH_2)_2(OAc)_4]$ wherein the macrocycle acts as a semiflexible ditopic ligand to coordinate pairs of metal ions *via* its indolenine N atoms into dinuclear metallocycles. The compounds LH_2, [Co(**L**)], and [Ni(**L**)] are isostructural and feature close π-stacking as well as linear chain arrangements in the case of the metal complexes. Variable temperature magnetic susceptibility measurements showed thermally induced paramagnetism in [Ni(**L**)].

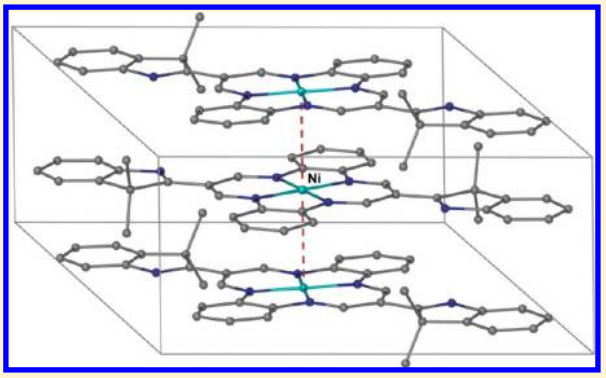

INTRODUCTION

Dibenzotetraaza[14]annulenes (TAAs) are a class of synthetic macrocyclic compounds that have attracted a great deal of continued interest since their introduction in 1969.[1−3] The attention on these compounds has been aroused mainly due to their resemblance to the naturally occurring porphyrins, thus their relevance in bioinorganic chemistry.

Similar to porphyrins, dibenzotetraaza[14]annulenes possess a number of double bonds in their framework and have four nitrogen atoms in a plane which can easily be deprotonated to generate dianionic ligands toward metal ions. However, in contrast to the fully delocalized aromatic ($4n + 2$) system of porphyrins, dibenzotetraaza[14]annulenes are Hückel antiaromatic ($4n$). Compared to the essentially rigid planar porphyrins, dibenzotetraaza[14]annulenes are more flexible and can adopt different conformations, varying between planar and so-called "saddle-shaped" conformations. For the free ligands, the planarity can persist when R^2 = H (Figure 1), whereas the β-substituted molecules ($R^2 \neq$ H) adopt a saddle-shaped conformation because of the steric interactions between the R^2 groups and the hydrogen atoms of *o*-phenylene rings. Another difference between dibenzotetraaza[14]annulenes and porphyrins concerns the smaller core size (defined as the average N-centroid distances) of the former by about 0.1 Å.

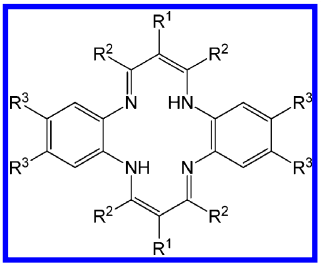

Figure 1. Dibenzotetraaza[14]annulenes.

The template synthesis of dibenzotetraaza[14]annulenes consists of 2:2 condensation of an *o*-phenylene diamine and a 1,3-dicarbonyl in the presence of Ni^{II} ion.[1,4] The metal ion can then be removed from the macrocycle using hydrochloric acid to give the free ligand. Without coordinating assistance of the metal ion, a 1:1 condensation reaction often occurs to form the 1,5-benzodiazepine (Scheme 1). Exceptions occur for 1,3-dialdehyde precursors bearing electron withdrawing groups Br, CN, and pyridine at the α-positions, where the 2:2 condensations generate the corresponding *meso*-susbstituted tetraaza macrocycles.[5,6] The other nontemplate methods for

Received: October 3, 2012
Published: January 30, 2013

   dx.doi.org/10.1021/ic302150j | *Inorg. Chem.* 2013, 52, 1926−1941

Scheme 1. Synthesis of Dibenzotetraaza[14]annulenes *vs* 1,5-Benzodiazepines

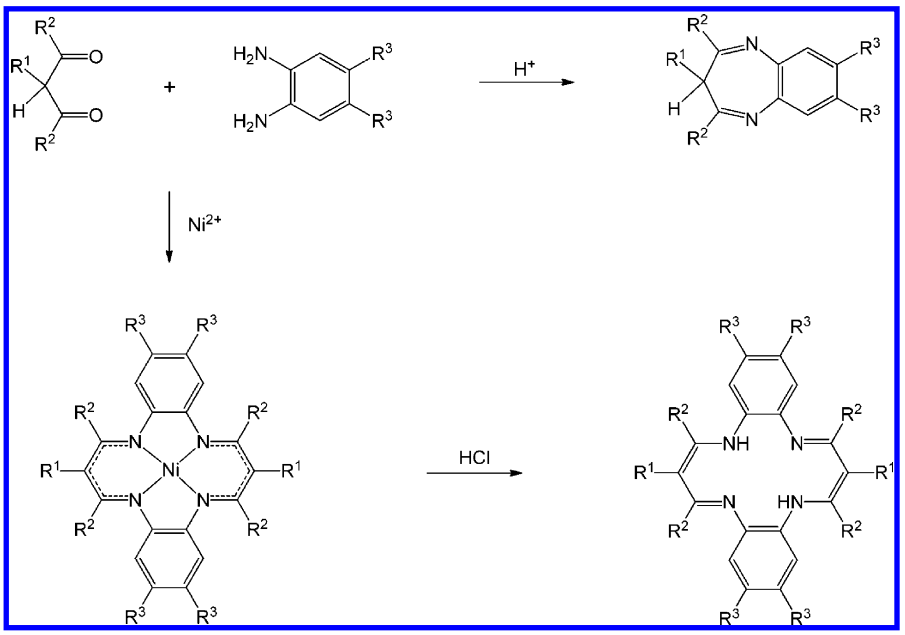

Scheme 2. Synthesis of LH_2

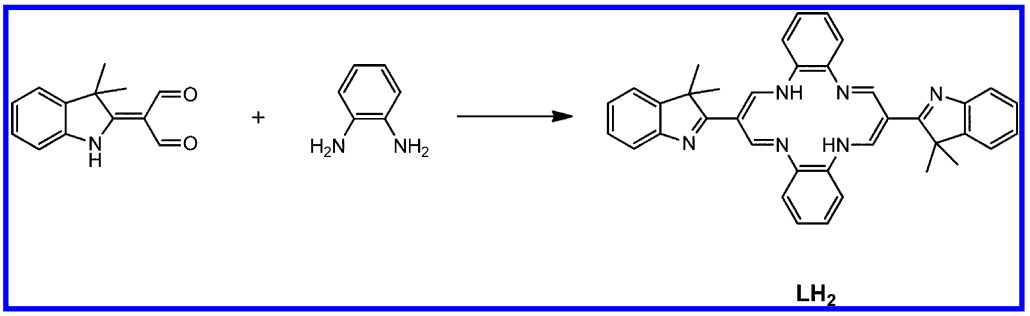

the synthesis of TAAs include the reactions of *o*-phenylene diamine with propynal[7,8] or substituted acroleins (e.g., 3-formylchromone and amino-2-nitroacroleine).[9−13]

Compared to the extensive research devoted to the coordination chemistry of *β*-substituted dibenzotetraaza[14]-annulenes, the *β*-unsubstituted analogues are relatively understudied. A search of the Cambridge Structural Database revealed that, to date, 248 dibenzotetraaza[14]annulene metal complexes have been crystallographically characterized, but only 21 of those are for *β*-unsubstituted TAAs.[14] In this paper a new *β*-unsubstituted dibenzotetraaza[14]annulene, bearing two 3,3-dimethylindolenine fragments at the *meso* positions, thus rich in *π*-delocalized areas, is introduced as a ligand for transition metals. The presence of the electron withdrawing imine groups at the *meso* positions not only enhances the reactivity of the axial coordination sites of the tetraaza metal complexes, but also offers new potential coordinating sites, i.e., the indolenine N atoms. In addition, the extension of the *π*-system to the indolenine rings provides additional possibilities for *π*-involved interactions (*π*···*π*, X−H···*π*, and metal···*π*), which can have prominent influences on determining the supramolecular topology.

RESULTS AND DISCUSSION

Synthesis and Structure of the Free Ligand. The synthesis of the indolenine substituted dibenzotetraaza[14]-annulene was achieved through the 2:2 condensation of 2-(diformylmethylidene)-3,3-dimethylindole with *o*-phenylenediamine accompanied by migration of the double bond into the pyrrole rings. According to the template synthesis, the macrocyclization would need assistance of metal coordination; however, we were surprised to find out that the reaction in the absence of a metal ion proceeded to generate the desired 14-membered macrocycle, LH_2, in 81% yield (Scheme 2). The inconsistency with the general observation of 1,5-benzodiazepine formation in the analogous reactions might be attributed to the electron-withdrawing effect of the imine functional group (*vide supra*).

The ^{1}H NMR spectrum of LH_2 shows the six protons of the 14-membered tetraaza ring as a triplet at δ = 14.58 ppm (J = 6.1 Hz) for the two internal N*H* and a doublet with the same coupling constant at 8.95 ppm for the four C*H*N protons. This is characteristic for such a ring system and has been explained in terms of rapid imine-enamine tautomerism.[15] The 12 methyl hydrogens appear as a singlet at δ = 1.60 ppm.

Figure 2 shows the crystal structure of molecule LH_2. The asymmetric unit of the crystal consists of two-half molecules whose geometrical parameters differ only slightly; therefore only one molecule is depicted. The centers of the molecules lie at crystallographic centers of inversion in the triclinic space group $P\bar{1}$, translated by 1/2 along the crystallographic *a* direction. As expected for a *β*-unsubstituted TAA, the

dx.doi.org/10.1021/ic302150j | Inorg. Chem. 2013, 52, 1926−1941

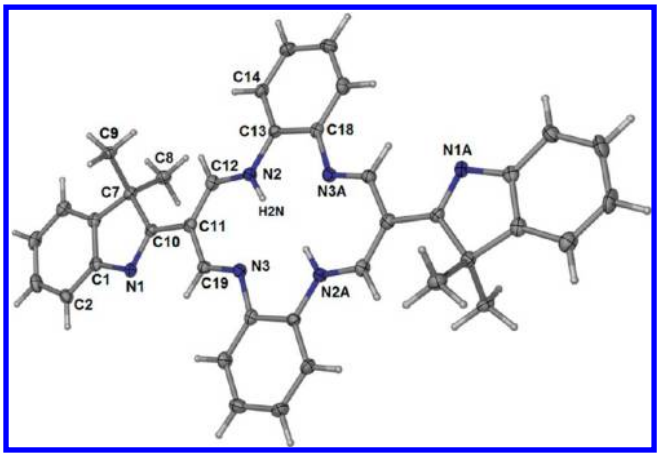

Figure 2. The molecular structure and atom labeling scheme of LH_2 (50% probability ellipsoids).

dibenzotetraaza[14] annulene system adopts a planar conformation. Interestingly, the two attached indolenine rings are coplanar with this system; thus the whole molecule (except for the methyl groups) lies in a plane [maximum deviation = 0.043(4) Å for C7], and the methyl groups lie on either side of the plane. In contrast, the planar dibenzotetraaza[14] annulenes with the *meso*-carbons linked to six-membered aromatic rings showed some degree of twist about the linkages.[16−19] The methyl hydrogens H8C and H9C are separated from the propanediiminato H atom, H12, by 2.17 and 2.12 Å respectively, which are shorter than the van der Waals sum (2.4 Å). Selected bond lengths and angles are listed in Table 1.

Table 1. Selected Bond Lengths (Å) and Bond Angles (°) for LH_2, $LH_2{\cdot}2CHCl_3$, and $LH_4^{2+}{\cdot}2Cl^-$[a]

	LH_2	$LH_2{\cdot}2CHCl_3$	$LH_4^{2+}{\cdot}2Cl^-$
Bond lengths			
N(1)−C(10)	1.305(5)	1.3056(18)	1.328(2)
N(2)−C(12)	1.341(5)	1.3365(18)	1.289(2)
N(2)−C(13)	1.392(5)	1.4056(17)	1.423(2)
N(3)−C(19)	1.290(5)	1.2942(18)	1.313(2)
N(3)−C(18)#1	1.423(5)	1.4213(18)	1.414(2)
C(10)−C(11)	1.467(6)	1.4606(19)	1.424(2)
C(11)−C(12)	1.366(6)	1.3834(19)	1.440(2)
C(11)−C(19)	1.441(6)	1.4496(19)	1.408(2)
Bond angles			
C(12)−N(2)−C(13)	127.3(4)	125.24(12)	118.23(14)
C(19)−N(3)−C(18)#1	119.3(3)	118.42(12)	126.63(15)
C(12)−C(11)−C(19)	122.5(4)	122.08(12)	121.51(15)
N(2)−C(12)−C(11)	124.7(4)	124.36(13)	125.22(15)
N(2)−C(13)−C(18)	117.5(4)	117.98(12)	117.52(14)
C(13)−C(18)−N(3)#1	116.4(3)	116.88(12)	117.44(15)
N(3)−C(19)−C(11)	125.5(4)	124.02(13)	122.94(16)

[a]Symmetry transformations used to generate equivalent atoms: #1 $-x+1, -y+1, -z+1$ (for LH_2); $-x+2, -y, -z+2$ (for $LH_2{\cdot}2CHCl_3$); $-x+2, -y+1, -z+1$ (for $LH_4^{2+}{\cdot}2Cl^-$).

The core size of the macrocycle ring is 1.93 Å, which falls within the expected range. The propanediiminato moiety (N2/C12/C11/C19/N3) exhibits substantial bond length alternation, indicative of incomplete π-delocalization within the linkage. This moiety is linked to the indolenine and benzene rings by nominally single C−C and C−N bonds, respectively.

Figure 3 displays the packing of the crystal structure. The planar molecules are stacked above each other in an antiparallel manner along the *a* axis, perpendicular to the molecular plane. The succeeding molecules along the stack are rotated by an angle of 23° and separated by 3.4285(5) Å. The packing is consolidated by C−H···N interactions formed between a methyl hydrogen and indolenine N atoms (see Supporting Information, Table S1).

The linear stacking arrangement observed here is unprecedented for a free TAA ligand and is obviously the effect of the two *meso*-placed dimethylindolenine substituents: the parent *meso*-unsubstituted TAA exhibits a herringbone pattern.[20] The characteristic needle-shaped crystals, with the *a* axis aligned along the needle axis, suggest that $\pi\cdots\pi$ and C−H···N interactions have a significant impact on crystal growth. The close stacking and the molecular planarity of LH_2 are, however, disrupted when the macrocycle is cocrystallized with chloroform solvent molecules. Figure 4 shows the crystal structure of the chloroform disolvate. In this structure, in the monoclinic space group $P2_1/n$, the macrocycle is situated at a crystallographic inversion center. Two chloroforms are positioned above the six-membered rings of the indolenine moieties so as to give strong C−H···π interactions (see Supporting Information, Table S1). As a result, the macrocycle has lost its planarity and adopts a step-like conformation, the r.m.s. deviation from the plane of the 14 atoms of the tetraaza ring being 0.105 Å. The indolenine ring is twisted by 7.08(6)° out of the plane of the attached propanediiminato fragment.

Table 1 lists the selected bond lengths and angles for $LH_2{\cdot}2CHCl_3$ and Figure 5 shows a packing view of the crystal structure. In the crystal, the macrocyclic molecules are connected into zigzag layers in (−1 0 1) plane *via* C−H···π and C−H···N interactions (see Supporting Information, Table S1).

The effect of protonation of the imine group at the *meso* positions on the crystal structure can be understood from the structure of the dichloride salt of the doubly protonated macrocycle $LH_4^{2+}{\cdot}2Cl^-$. The crystal structure of the salt is represented in Figure 6, and selected bond lengths and angles are given in Table 1. The center of the molecule resides on a crystallographic center of inversion and the chloride anions are hydrogen bonded to indolic nitrogen atoms. Comparison of the bond lengths of the neutral molecule, LH_2, to those of the dichloride salt, ($LH_4^{2+}{\cdot}2Cl^-$), reveals that the protonation of the indolenine nitrogen atoms is associated with shortening of the C10−C11 linkage, and lengthening of N1−C10. The dibenzotetraaza[14] annulene fragment remains almost planar with the r.m.s. deviation from the plane of its 22 non-H atoms being 0.0335 Å. The indolenine rings are rotated out of this plane by 8.86(5)°.

Figure 7 shows a packing view of the crystal structure, looking down the crystallographic *a* axis. In the crystal, the molecules are linked into infinite chains along the *c* axis through $\pi\cdots\pi$ interactions [centroid−centroid distance = 3.4631(10) Å] formed by the indolic six-membered rings of the molecules related by symmetry operation $-x+2, -y+1, -z$. The chains are further connected into a three-dimensional polymeric structure *via* C−H···π interactions (see Supporting Information, Table S1).

The molecular structure of the synthesized dibenzotetraaza[14]annulene, LH_2, offers two types of metal coordination site, namely, the central cavity and the indolenine nitrogen atoms. The coordination behavior of LH_2, toward

dx.doi.org/10.1021/ic302150j | Inorg. Chem. 2013, 52, 1926−1941

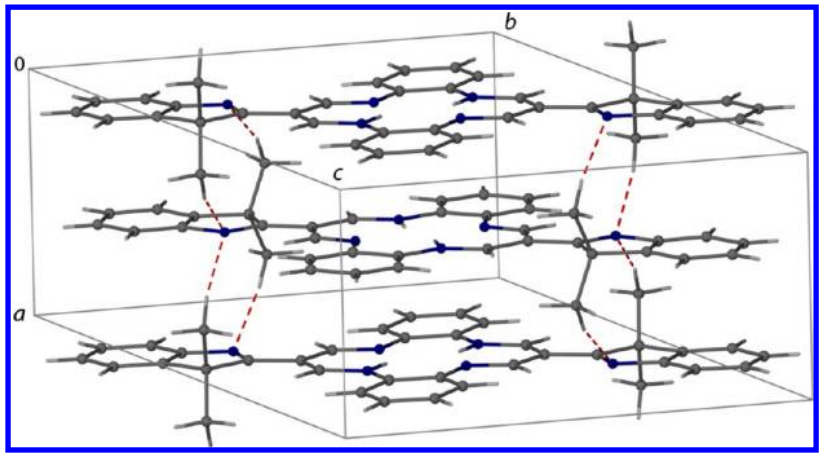

Figure 3. Packing view of LH_2. C−H···N hydrogen bonds are depicted as red dashed lines.

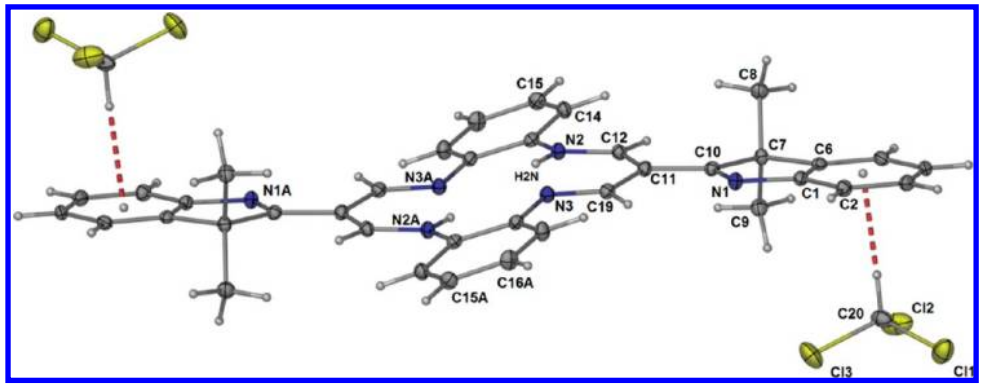

Figure 4. The molecular structure and atom labeling schemes of $LH_2{\cdot}2CHCl_3$ (50% probability ellipsoids).

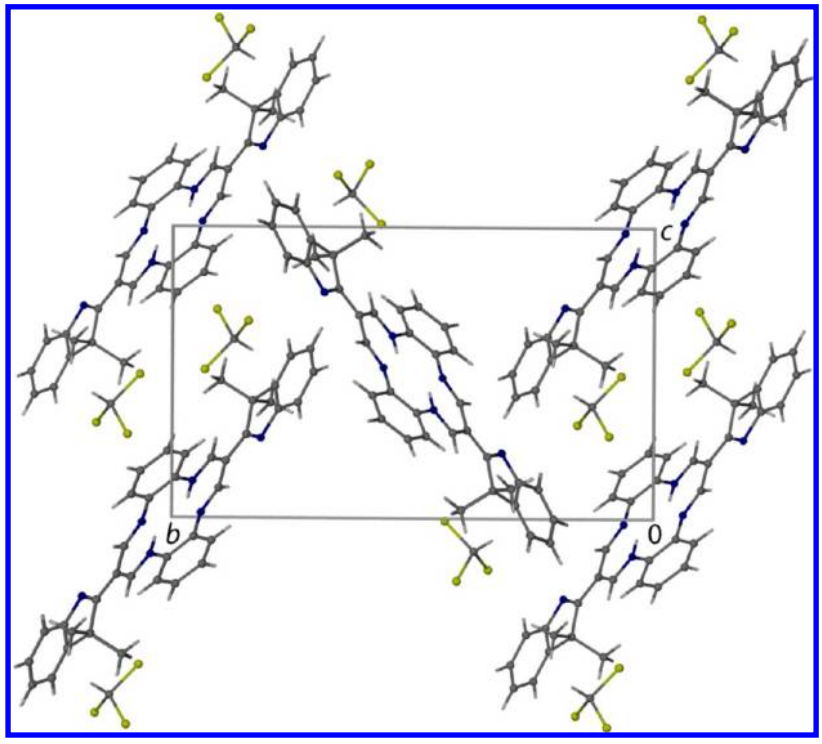

Figure 5. Packing view of $LH_2{\cdot}2CHCl_3$, looking down the *a* axis.

different transition metal ions, was then studied. The reactions with Co^{II}, Ni^{II}, Cu^{II}, and Pd^{II} ions gave the metal complexes in moderate to high yield, whereas the Mn^{III}, Fe^{III} complexes could be obtained only as few X-ray quality crystals.

dx.doi.org/10.1021/ic302150j | *Inorg. Chem.* 2013, 52, 1926−1941

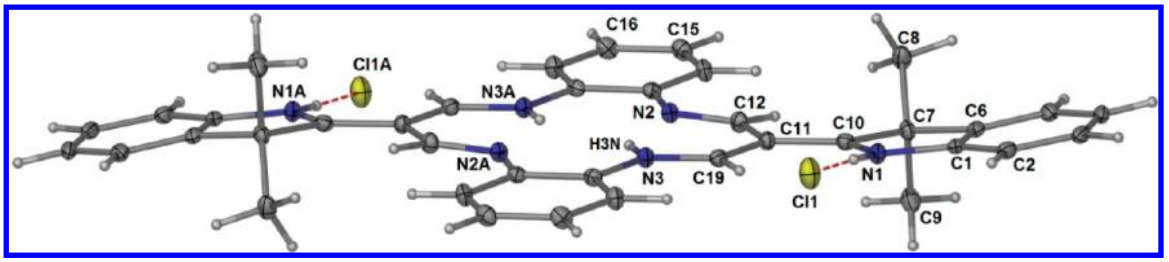

Figure 6. The molecular structure and atom labeling schemes of $\mathbf{L}H_4^{2+}\cdot 2Cl^-$ (50% probability ellipsoids).

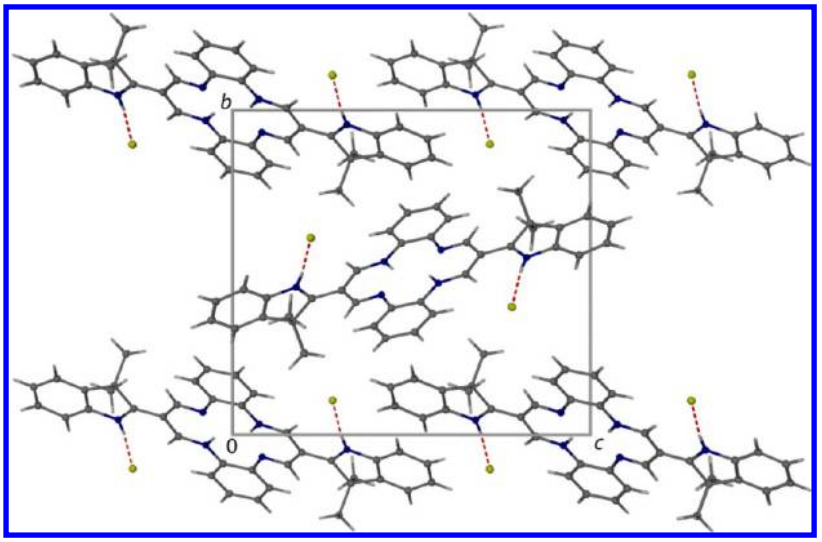

Figure 7. Packing view of $\mathbf{L}H_4^{2+}\cdot 2Cl^-$ looking down the *a* axis.

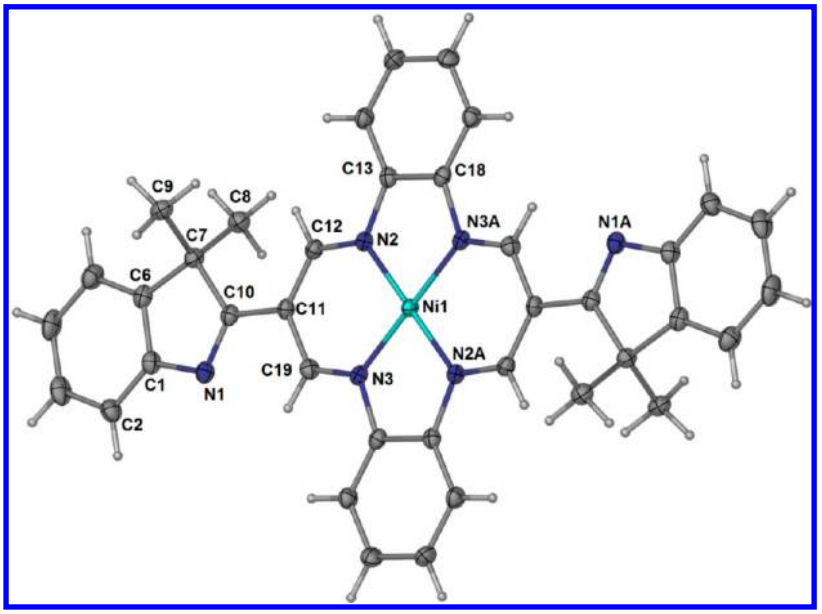

Figure 8. The molecular structure and atom labeling scheme of [Ni(**L**)] (50% probability ellipsoids).

Structure of the Nickel(II) Complex. The reaction of the ligand with nickel(II) acetate afforded thin red needles of the product [Ni(**L**)]. In the ^{1}H NMR spectrum of the nickel complex the N*H* resonance of the ligand no longer exists, and the resonance of the four C*H*N protons of the propanediiminato moieties appears as a singlet at δ = 8.81 ppm. The X-ray crystallographic analysis shows that the crystal structure of the nickel(II) complex is isomorphous with that of the neutral free ligand. A stacked, linear chain of the metal ions results from the placement of the nickel(II) ion within the central cavity. The asymmetric unit consists of two half-molecules, separated by 1/2 *a*, with very similar geometrical parameters. The structure of one molecule is exhibited in Figure 8. The nickel(II) complex, [Ni(**L**)], is essentially planar (except for the methyl groups) with a maximum deviation from the plane of 0.045(3) Å for C7. Table 2 compiles selected bond lengths and

dx.doi.org/10.1021/ic302150j | *Inorg. Chem.* 2013, 52, 1926−1941

Table 2. Selected Bond Lengths (Å) and Bond Angles (°) for [Ni(L)][a]

Bond lengths			
Ni(1)−N(3)	1.858(3)	N(3)−C(19)	1.314(4)
Ni(1)−N(2)	1.867(3)	N(3)−C(18)#1	1.423(4)
N(1)−C(10)	1.297(4)	C(10)−C(11)	1.471(4)
N(2)−C(12)	1.325(4)	C(11)−C(12)	1.387(4)
N(2)−C(13)	1.417(4)	C(11)−C(19)	1.411(4)
Bond angles			
N(3)−Ni(1)−N(2)#1	85.73(11)	N(2)−C(12)−C(11)	125.4(3)
C(12)−N(2)−C(13)	119.8(3)	C(18)−C(13)−N(2)	113.4(3)
C(19)−N(3)−C(18)#1	119.4(3)	C(13)−C(18)−N(3)#1	113.3(3)
C(12)−C(11)−C(19)	121.6(3)	N(3)−C(19)−C(11)	125.4(3)

[a]Symmetry transformations used to generate equivalent atoms: #1 $-x + 1, -y + 1, -z + 1$.

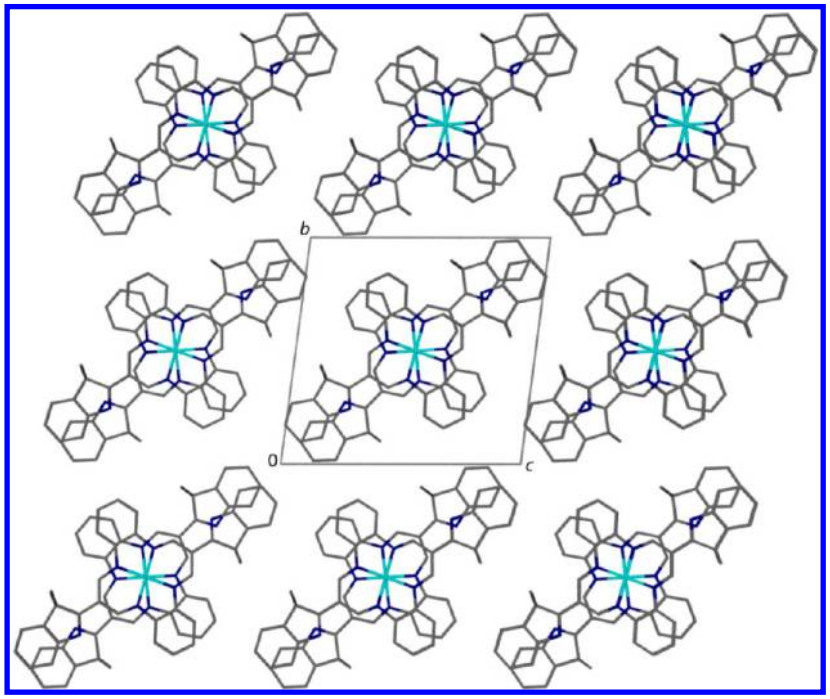

Figure 9. Packing view of structure [Ni(**L**)] looking down the *a* axis.

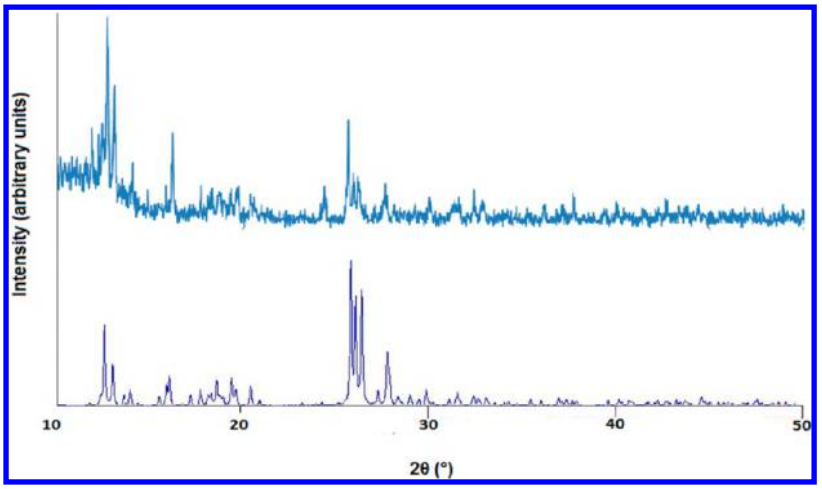

Figure 10. Qualitative comparison of experimental powder diffraction pattern of [Co(**L**)] (top) with simulated pattern based on the single-crystal structure of [Ni(**L**)] (bottom).

angles. The average Ni−N distance of 1.862 Å is shorter than the average nitrogen-to-center distance, N−Ct, of the neutral free ligand (1.93 Å) because increased delocalization and contraction is associated with the loss of the two amino hydrogens, as discussed by Goedken et al.[21] The contraction is reflected in the total angular decrease of the ten interior and

dx.doi.org/10.1021/ic302150j | *Inorg. Chem.* 2013, 52, 1926−1941

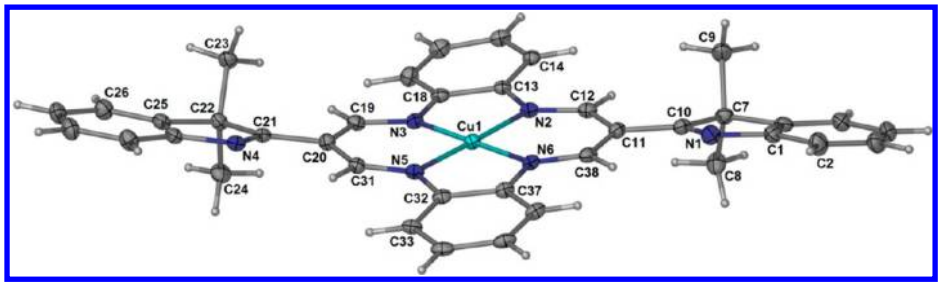

Figure 11. The molecular structure and atom labeling scheme of [Cu(**L**)] (50% probability ellipsoids). Acetic acid solvate molecules are not shown.

Table 3. Selected Bond Lengths (Å) and Bond Angles (°) for [Cu(L)]

Bond lengths			
Cu(1)−N(2)	1.919(2)	N(5)−C(31)	1.302(4)
Cu(1)−N(3)	1.910(2)	N(5)−C(32)	1.418(4)
Cu(1)−N(5)	1.917(2)	N(6)−C(38)	1.295(4)
Cu(1)−N(6)	1.932(2)	N(6)−C(37)	1.411(3)
N(1)−C(10)	1.303(4)	C(10)−C(11)	1.460(4)
N(2)−C(12)	1.314(4)	C(11)−C(12)	1.406(4)
N(2)−C(13)	1.399(4)	C(11)−C(38)	1.414(4)
N(3)−C(19)	1.323(4)	C(19)−C(20)	1.404(4)
N(3)−C(18)	1.406(4)	C(20)−C(31)	1.410(4)
N(4)−C(21)	1.303(4)	C(20)−C(21)	1.461(4)
Bond angles			
N(3)−Cu(1)−N(5)	94.74(10)	C(12)−C(11)−C(38)	124.0(3)
N(3)−Cu(1)−N(2)	84.73(11)	N(2)−C(12)−C(11)	125.9(3)
N(5)−Cu(1)−N(2)	178.83(11)	N(2)−C(13)−C(18)	115.0(2)
N(3)−Cu(1)−N(6)	179.84(12)	N(3)−C(18)−C(13)	114.1(3)
N(5)−Cu(1)−N(6)	85.41(11)	N(3)−C(19)−C(20)	125.4(3)
N(2)−Cu(1)−N(6)	95.12(10)	C(19)−C(20)−C(31)	123.8(3)
C(12)−N(2)−C(13)	122.9(2)	N(5)−C(31)−C(20)	125.3(3)
C(19)−N(3)−C(18)	121.4(3)	C(37)−C(32)−N(5)	115.3(2)
C(21)−N(4)−C(30)	106.9(2)	C(32)−C(37)−N(6)	114.9(2)
C(38)−N(6)−C(37)	122.8(3)	N(6)−C(38)−C(11)	125.5(3)

four exterior angles of the tetraazaannulene by 30.4°. The short Ni−N bond distance is consistent with what has previously been observed for Ni complexes of TAAs and highlights the difference in cavity size between TAAs and porphyrins as well as the ability of nickel(II) to adjust its covalent radius. For comparison, the average 4-coordinate Ni−N(porphyrin) distance is 1.933 Å in 469 observations, whereas the average Ni−N(TAA) distance is 1.863 Å in 51 observations in the Cambridge Structural Database.[14] Figure 9 depicts a packing projection of the nickel complex, looking down the *a* axis. The planar molecules are stacked in an antiparallel fashion on top of each other (staggered by 22°) with their Ni^{II} atoms aligned along the stack direction, separated by a distance of 3.448(2) Å. This packing structure is similar to the well-known structure of $Ni(dmg)_2$ with Ni−Ni separation of 3.25 Å.[22,23] Among the dibenzotetraaza[14]annulenes complexes, only the partially oxidized forms of the Ni^{II}, Cu^{II}, Pd^{II}, and Pt^{II} complexes of the prototype TAA ligand show linear chain stacking patterns with metal−metal distances of 3.175−3.250 Å.[24] Moreover, the saddle-shaped structure of [Ni(Cl_4Me_4TAA)] shows Ni−Ni distances of 3.3860(11) and 3.5888(11) Å in two different dimers in the asymmetric unit.[25] The unoxidized Ni^{II} complex of the unsubstituted TAA[26] crystallizes in a slipped stack structure with no proximate metal···metal distances.

Structure of the Cobalt(II) Complex. The [Co(**L**)] complex was prepared in a similar manner as for the analogous Ni complex. Our attempts to grow X-ray quality single crystals of this compound were unsuccessful; however the XRD pattern of the pristine [Co(**L**)] (Figure 10) matches well with the simulated powder patterns based on the single crystal structure of [Ni(**L**)] (calculated using Mercury).[27] Furthermore, small single crystals were obtained from a mixture of the Co complex and the free macrocycle. Determination of the crystal structure revealed it to be isostructural with [Ni(**L**)] and LH_2. In the mixed crystal, the occupancies of the Co atoms in the two half-molecules of the unit cell were refined to 0.75 and 0.71. Although the structure is occupationally disordered, the intermolecular center-to center distance (1/2 *a*) of 3.421(3) Å indicates a metal···metal distance similar to that of the [Ni(**L**)] complex. Also, the average Co−N distance of 1.867 Å is in agreement with the average value of 1.873 Å found in the orthorhombic slipped stack structure of square planar, unsubstituted [Co(TAA)].[28]

Structure of the Copper(II) Complex. The molecular structure of the copper(II) complex, [Cu(**L**)].0.5AcOH, is shown in Figure 11. The structure is noncentrosymmetric and the metal ion is located on a general position. A comparison with the structure of the free ligand reveals that a rotation about the propanediiminato-indolenine C−C linkage has occurred; thus the two indolenine N atoms in [Cu(**L**)] have a *cis*-orientation. The 14-membered macrocycle atoms deviate by up to 0.138(3) Å (for C20) from planarity, and the two indolenine rings are twisted in the same direction with respect to this plane by 14.86(8)° and 15.58(8)° about C10−C11 and C20−C21

dx.doi.org/10.1021/ic302150j | *Inorg. Chem.* 2013, 52, 1926−1941

respectively. Consequently, the methyl and diiminato hydrogen atoms, H9C and H12, are brought close together (1.98 Å) as are H23C and H19 (2.01 Å). The selected bond lengths and angles are given in Table 3. The average Cu−N distance of 1.920 Å is comparable to those observed in similar systems,[28−30] but longer than the average Ni−N distance of 1.862 Å in [Ni(**L**)]. When compared to the Ni^{II} complex, the metal−nitrogen lengthening of the Cu^{II} complex is accompanied by expansion of the 14-membered ring as deduced from the total angular increase of the 14 angles of the ring by 22.7°. The Cu^{II} atom is almost perfectly in the [N_4] plane with the displacement of 0.0091(3) Å.

In the crystal, the five-membered chelate rings are in slipped-parallel position with respect to the benzene rings of the adjacent molecules to form two metal-π interactions with alternate Cu···centroid distances of 3.482 and 3.422 Å (Figure 12). The molecules are stacked along the *a* axis with the

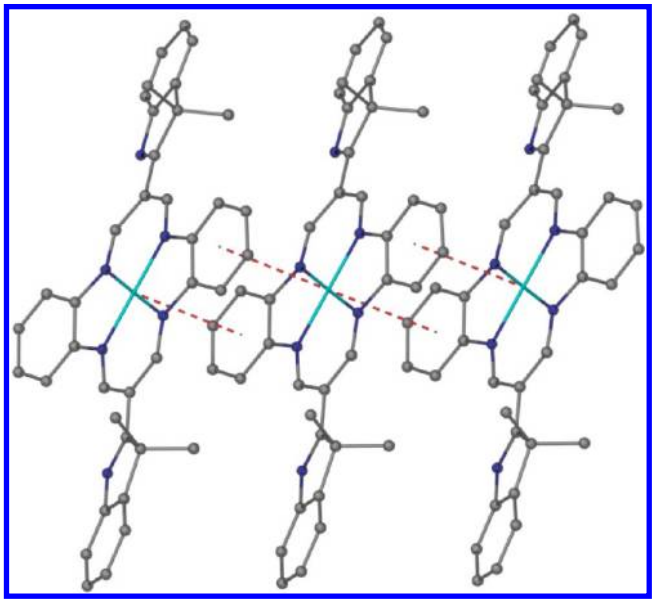

Figure 12. Cu···π interactions in [Cu(**L**)] forming infinite chains along the *a* axis.

Cu···Cu distance (5.8858(10) Å) corresponding to the *a*-periodicity. The chains are further connected *via* C−H···π interactions (see Supporting Information, Table S2 and Figure S1) to form zigzag layers parallel to the *ab* plane. The arrangement of the adjacent zigzag layers in the crystal leads to the formation of channels along the *a* axis (void size = 117 $Å^3$). The voids contain acetic acid solvent molecules which act as H-bond donors to N1.

Structure of the Manganese(III) Complexes. The reaction of the ligand with $MnBr_2$ accompanied by aerial oxidation of Mn^{II} to Mn^{III} gave a few X-ray quality crystals of [Mn(**L**)Br]·0.6CH_3OH·0.4H_2O. As shown in Figure 13, the metal atom is coordinated by the [N_4] donor set and an apically placed Br atom in a square pyramidal geometry. The average N−Ct is 1.91 Å while the average of the Mn−N bond lengths is 1.951 Å. The difference between the available core size and the Mn−N distances is adjusted by displacement of the metal by 0.3988(12) Å from the [N_4] plane toward the Br atom. Consequently, the C−N bonds in the five- and six-membered chelate rings are twisted by up to 17.2(4)° (Table 4) to direct the [N_4] lone pairs toward the metal atom. The 14-membered tetraaza ring atoms deviate by up to 0.223(2) Å (for C11) from planarity. The planes of the nine-membered indolenine rings and the attached propanediiminato moieties are twisted with respect to each other by 18.93(12)° and 14.40(12)° about C10−C11 and C20−C21 respectively, resulting in short H12···H9B (1.942 Å) and H31···H24B (2.035 Å) contacts.

In a similar way, crystals of [Mn(**L**)Cl]·$CHCl_3$ were obtained and showed a structure comparable to that of [Mn(**L**)Br] (Figure 14). The Mn(III) atom lies 0.3896(13) Å out of the [N4] plane and the torsion angles about the tetraaza ring C−N bonds varies between 0.8(3) and 10.4(5)° (Table 5). The 14-membered tetraaza ring deviates less from planarity (maximum deviation = 0.108 (2) Å for N6) than that in the Br-coordinated analogue. The two indolenine nitrogens are at the same side of the molecule (unlike the structure of [Mn(**L**)Br]) and the N1 and N4 containing indolenine rings make dihedral angles of 19.02(13) and 10.41(14)° with the attached propanediiminato moieties, respectively.

Mn complexes of the β-unsubstituted dibenzotetraaza[14]-annulenes are unprecedented; however the square-pyramidal high spin Mn(III) complexes of the prototype saddle-shaped dibenzotetraaza[14]annulene, [Mn(Me_4TAA)Cl] and [Mn-(Me_4TAA)NCS],[31,32] have Mn−N bond lengths similar to those of the present structures. The Mn−Cl distance of 2.3654(10) Å is comparable to that in [Mn(Me_4TAA)Cl], and the Mn−Br distance of 2.5067(6) Å is similar to the corresponding value in tetraphenylporphyrinatomanganese(III) bromide,[33] the closest analogous structure.

The crystal network of [Mn(**L**)Br] contains disordered solvent methanol and water molecules, hydrogen bonded to the indolenine N4 atom. In the crystal, the metal complex molecules are bonded to a 3D-supramolecular network through C−H···Br and C−H···π interactions (see Supporting Information, Table S2). Similarly, in the crystal of [Mn(**L**)Cl] the metal complex molecules are connected through C−H···Cl and C−H···π interactions into a 3D network wherein solvent chloroform molecules are trapped (Figure 15). The chloroform

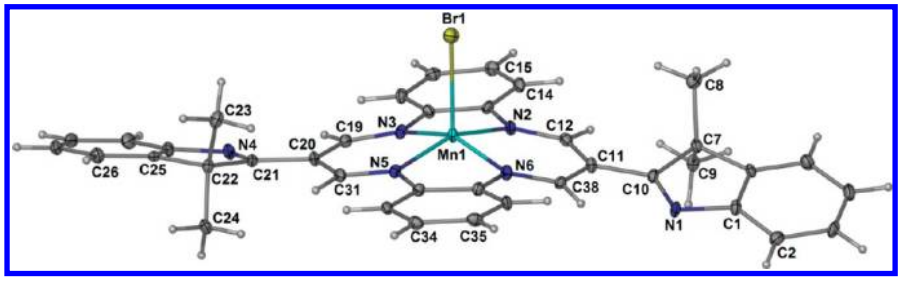

Figure 13. The molecular structure of [Mn(**L**)Br] showing the atom labeling scheme (50% probability ellipsoids). The solvate molecules are not shown.

dx.doi.org/10.1021/ic302150j | *Inorg. Chem.* 2013, 52, 1926−1941

Table 4. Selected Bond Lengths (Å), Bond Angles (°) and Torsion Angles (°) for [Mn(L)Br]

Bond lengths			
Mn(1)−Br(1)	2.5067(6)	N(5)−C(31)	1.326(3)
Mn(1)−N(2)	1.942(2)	N(5)−C(32)	1.431(3)
Mn(1)−N(5)	1.946(2)	N(6)−C(38)	1.304(3)
Mn(1)−N(3)	1.955(2)	N(6)−C(37)	1.429(4)
Mn(1)−N(6)	1.962(2)	C(10)−C(11)	1.465(4)
N(1)−C(10)	1.300(4)	C(11)−C(12)	1.398(4)
N(2)−C(12)	1.334(3)	C(11)−C(38)	1.410(4)
N(2)−C(13)	1.420(4)	C(19)−C(20)	1.416(4)
N(3)−C(19)	1.313(3)	C(20)−C(31)	1.395(4)
N(3)−C(18)	1.432(3)	C(20)−C(21)	1.470(4)
N(4)−C(21)	1.297(3)		
Bond angles			
N(2)−Mn(1)−N(5)	158.30(10)	C(31)−N(5)−C(32)	122.0(2)
N(2)−Mn(1)−N(3)	82.81(10)	C(38)−N(6)−C(37)	122.4(2)
N(5)−Mn(1)−N(3)	92.27(9)	C(12)−C(11)−C(38)	123.4(2)
N(2)−Mn(1)−N(6)	91.87(10)	N(2)−C(12)−C(11)	125.5(3)
N(5)−Mn(1)−N(6)	83.52(10)	C(18)−C(13)−N(2)	114.3(2)
N(3)−Mn(1)−N(6)	154.52(10)	C(13)−C(18)−N(3)	114.3(2)
N(2)−Mn(1)−Br(1)	101.78(7)	N(3)−C(19)−C(20)	125.7(3)
N(5)−Mn(1)−Br(1)	99.91(7)	C(31)−C(20)−C(19)	123.7(2)
N(3)−Mn(1)−Br(1)	104.81(7)	N(5)−C(31)−C(20)	124.9(3)
N(6)−Mn(1)−Br(1)	100.67(7)	C(37)−C(32)−N(5)	114.7(2)
C(12)−N(2)−C(13)	121.2(2)	C(32)−C(37)−N(6)	115.1(2)
C(19)−N(3)−C(18)	122.1(2)	N(6)−C(38)−C(11)	125.4(3)
Torsion angles			
C(13)−N(2)−C(12)−C(11)	6.4(3)	C(32)−N(5)−C(31)−C(20)	1.2(3)
C(12)−N(2)−C(13)−C(14)	15.3(4)	C(31)−N(5)−C(32)−C(33)	7.3(4)
C(19)−N(3)−C(18)−C(17)	4.3(4)	C(38)−N(6)−C(37)−C(36)	17.2(4)
C(18)−N(3)−C(19)−C(20)	2.6(3)	C(37)−N(6)−C(38)−C(11)	3.6(3)

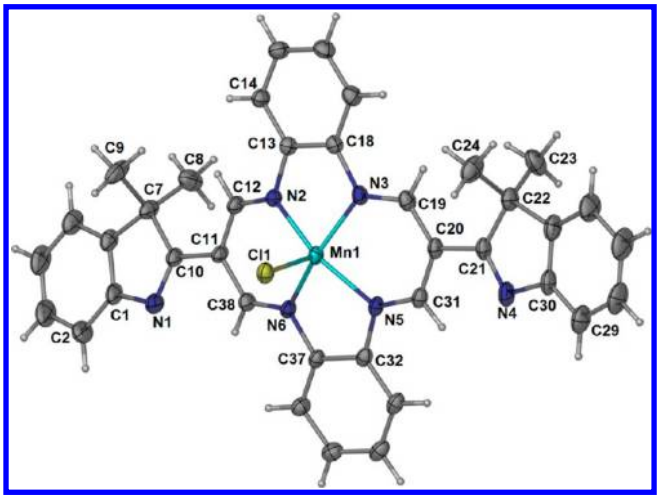

Figure 14. The molecular structure of [Mn(**L**)Cl] showing the atom labeling scheme (30% probability ellipsoids). Chloroform solvate molecules are not shown.

acts as an H-bond donor to the Cl ligands (see Supporting Information, Table S2). In addition, metal-π interactions (3.862 Å) are observed between the Mn(III) and the C32−C37 ring of the symmetry related molecule forming centrosymmetric dimers.

Structure of the Iron(III) Complex. The reaction of the ligand with $FeCl_2$, accompanied by the oxidation of Fe^{II} to Fe^{III}, provided a few crystals of the cationic iron(III) complex of $[Fe(\mathbf{L}H_2)Cl_2]^+$ as the chloride salt, $[Fe(\mathbf{L}H_2)Cl_2]^+\cdot Cl^-\cdot CHCl_3$ (Scheme 3).

The crystal structure of the complex is shown in Figure 16 and the selected bond lengths and angles are listed in Table 6. As is reflected in the bond lengths of the iron(III) complex when compared to those of $\mathbf{L}H_2$, the ligand underwent imine-enamine tautomerism upon complexation with the metal ion; thus the indolic N atom is protonated. The metal ion is octahedrally coordinated by the core $[N_4]$ set and two axially located Cl atoms in a centrosymmetric structure. The electroneutrality is achieved by chloride anions, being placed on 2-fold rotation axes, connecting the neighboring cations into chains in [1 0 1] direction *via* N−H···Cl interactions (see Supporting Information, Table S2). The 14-membered tetraaza ring is essentially planar with an r.m.s. deviation of 0.034 Å and makes a dihedral angle of 7.57(9)° with the nine-membered indolic ring. Although the iron (II/III) complexes of β-substituted TAAs are known, the β-unsubstituted analogues are not. The average $Fe-N_{eq}$ distance of 1.916 Å is in the range for octahedral low-spin Fe^{III} complexes of similar ligands,[34,35] and shorter than in high-spin [Fe(Me$_4$TAA)Cl] with average lengths of 2.002 Å.[36] The Fe−Cl distance of 2.3251 Å is 0.07 Å longer than that in five-coordinate [Fe(Me$_4$TAA)Cl], the only known chloride adduct of an iron dibenzotetraaza[14]-annulene complex. Packing of the complex cations in the crystal forms channels along the *c*-axis (void size = 396 Å^3) wherein the chloride anions and the solvent chloroform molecules are trapped (Figure 17). The chloroform molecules act as H-bond donors to the axial Cl ligands and as acceptors in C−H···Cl bonds (see Supporting Information, Table S2).

dx.doi.org/10.1021/ic302150j | *Inorg. Chem.* 2013, 52, 1926−1941

Table 5. Selected Bond Lengths (Å), Bond Angles (°), and Torsion Angles (°) for [Mn(L)Cl]

Bond lengths			
Mn(1)−Cl(1)	2.3654(10)	N(5)−C(31)	1.318(4)
Mn(1)−N(3)	1.950(3)	N(5)−C(32)	1.422(4)
Mn(1)−N(6)	1.953(3)	N(6)−C(38)	1.320(4)
Mn(1)−N(2)	1.955(2)	N(6)−C(37)	1.422(4)
Mn(1)−N(5)	1.966(2)	C(10)−C(11)	1.472(4)
N(1)−C(10)	1.291(4)	C(11)−C(38)	1.388(4)
N(2)−C(12)	1.318(4)	C(11)−C(12)	1.391(4)
N(2)−C(13)	1.420(4)	C(19)−C(20)	1.386(5)
N(3)−C(19)	1.322(4)	C(20)−C(31)	1.400(5)
N(3)−C(18)	1.416(4)	C(20)−C(21)	1.481(4)
N(4)−C(21)	1.291(4)		
Bond angles			
N(3)−Mn(1)−N(6)	157.98(11)	C(31)−N(5)−C(32)	122.8(3)
N(3)−Mn(1)−N(2)	83.53(10)	C(38)−N(6)−C(37)	121.8(3)
N(6)−Mn(1)−N(2)	91.91(10)	C(38)−C(11)−C(12)	123.3(3)
N(3)−Mn(1)−N(5)	92.13(11)	N(2)−C(12)−C(11)	126.0(3)
N(6)−Mn(1)−N(5)	83.33(11)	C(18)−C(13)−N(2)	115.1(3)
N(2)−Mn(1)−N(5)	156.06(10)	C(13)−C(18)−N(3)	114.9(3)
N(3)−Mn(1)−Cl(1)	99.74(8)	N(3)−C(19)−C(20)	127.1(3)
N(6)−Mn(1)−Cl(1)	102.27(8)	C(19)−C(20)−C(31)	122.9(3)
N(2)−Mn(1)−Cl(1)	101.80(8)	N(5)−C(31)−C(20)	126.0(3)
N(5)−Mn(1)−Cl(1)	102.14(8)	C(37)−C(32)−N(5)	115.1(3)
C(12)−N(2)−C(13)	122.3(3)	C(32)−C(37)−N(6)	114.6(3)
C(19)−N(3)−C(18)	123.0(3)	N(6)−C(38)−C(11)	126.2(3)
Torsion angles			
C(13)−N(2)−C(12)−C(11)	1.6(3)	C(32)−N(5)−C(31)−C(20)	3.6(3)
C(12)−N(2)−C(13)−C(14)	9.1(5)	C(31)−N(5)−C(32)−C(33)	1.5(5)
C(19)−N(3)−C(18)−C(17)	7.1(5)	C(38)−N(6)−C(37)−C(36)	10.5(5)
C(18)−N(3)−C(19)−C(20)	0.8(3)	C(37)−N(6)−C(38)−C(11)	6.1(3)

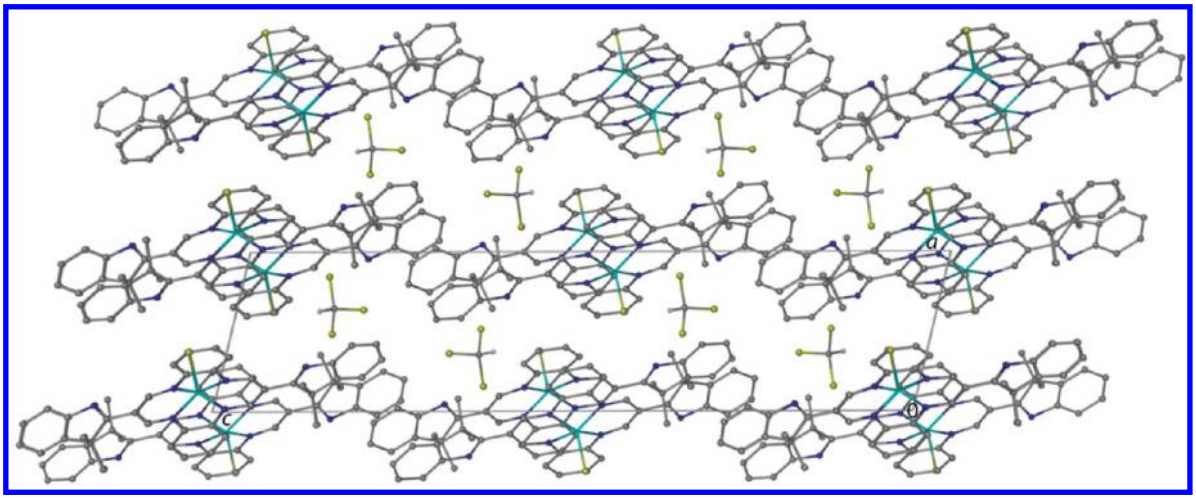

Figure 15. A packing view of [Mn(L)Cl].$CHCl_3$ looking down the *b* axis. Hydrogen atoms, except those for the chloroform molecules are omitted.

Structure of the Palladium(II) Complex. The reaction of LH_2 with a larger metal ion, i.e., Pd^{II} led to the formation of $[Pd_2(LH_2)_2(OAc)_4]$ (Scheme 4).

As shown in Figure 18, the neutral macrocyclic ligand uses its indolenine nitrogen atoms to coordinate to the Pd^{II} ions while its central core remains free. LH_2 thus functions as a ditopic ligand to doubly bridge pairs of Pd atoms into 26-membered metallocycles. Two *trans* located monodentate acetate ligands complete a square planar coordination environment around each palladium(II) ion. The ditopic macrocycle shows sufficient flexibility in forming the dimer so that the coordination geometry does not deviate too greatly from ideal square planar (Table 7). Thus, the two indolenine rings are in a *cis*-relationship and are rotated in a same direction out of the plane of the 14-membered tetraaza ring by 40.07(13) and 41.23(13)° about C10−C11 and C20−C21, respectively. As a result, the methyl hydrogens H9B and H23C are brought to distances of 2.03 and 1.97 Å from diiminato H12 and H19, respectively, effectively preventing the indolenine group from rotating by 90° to generate a larger intramolecular cavity. Within the dinuclear molecule, the metal centers are separated by 10.83 Å and the planes passing through the 14-membered tetraaza rings

dx.doi.org/10.1021/ic302150j | Inorg. Chem. 2013, 52, 1926−1941

Scheme 3. Synthesis of $[Fe(LH_2)Cl_2]^+ \cdot Cl^-$

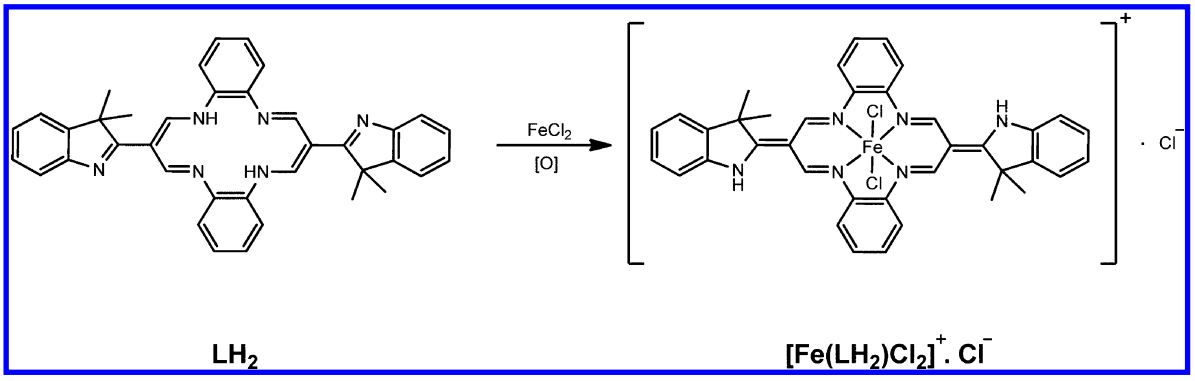

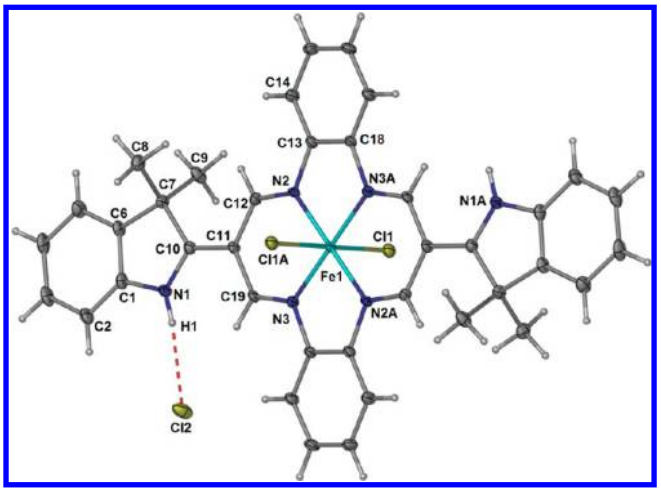

Figure 16. The molecular structure of $[Fe(LH_2)Cl_2]^+ \cdot Cl^-$ with thermal ellipsoids drawn at the 50% probability level. Chloroform solvate molecules are not shown.

(r.m.s. deviation = 0.108 Å; maximum deviation = 0.190(6) Å for C11) are separated by a distance of 3.32 Å.

Figure 19 represents a packing view of the crystal structure looking down the *c* axis. In the crystal, the adjacent dimers are connected through C−H···O and C−H···π interactions (see Supporting Information, Table S2) to form zigzag sheets in the *bc* plane. The arrangement of these layers along the *a* axis gives rise to a lattice with large voids (765 Å^3) within which there is no evidence for included solvent.

Magnetism of the Nickel(II) Complex. Since the crystal structure of [Ni(**L**)] shows a Ni···Ni separation of 3.448(2) Å in an extended linear chain as well as close $\pi\cdots\pi$ stacking between antiaromatic macrocycles, an unusual magnetism might be expected. Although the complex is EPR silent at 10 K and 25 K, variable temperature susceptibility measurements revealed that the complex has nonzero paramagnetism. As shown in Figure 20, the plot of $1/\chi$m approximates temperature independent paramagnetism over the range of *ca.* 20−300 K, but a sharp transition to antiferromagnetism occurs at a Néel temperature of 13 K. The plot of μ_{eff} shows an increase from 0.56 to 1.65 μ_B over the range 20−300 K, suggesting that the compound has a thermal population of a triplet excited state with a singlet ground state. This can arise, for example, when there is a small energy gap between a singlet ground state and triplet excited state, and has been proposed to occur in antiaromatic, planar, benzenoid polycyclic dianions.[37] Further study of the magnetic phenomena of the nickel(II) as well as of the isostructural cobalt(II) complex is planned.

CONCLUSIONS

Diindoleninyldibenzotetraaza[14]annulene, LH_2, obtained in a high yield through nontemplate dicarbonyl-diamine condensation, showed a whole molecule planarity and a linear chain stacking arrangement. The synthetic advantage and the unique crystal packing style would appear to be the effect of the indolenine substituents at the *meso* positions. The molecular planarity and the stacking pattern were disrupted by the presence of chloroform solvent molecules in the lattice or protonation of the indolenine N atoms. LH_2 offers two types of

Table 6. Selected Bond Lengths (Å) and Bond Angles (°) for $[Fe(LH_2)Cl_2]^+ \cdot Cl^-$[a]

Bond lengths			
Fe(1)−Cl(1)	2.3251(7)	N(3)−C(19)	1.295(4)
Fe(1)−N(2)	1.915(2)	N(3)−C(18)#1	1.437(3)
Fe(1)−N(3)	1.917(2)	C(10)−C(11)	1.418(4)
N(1)−C(10)	1.333(4)	C(11)−C(12)	1.425(4)
N(2)−C(12)	1.304(4)	C(11)−C(19)	1.442(4)
N(2)−C(13)	1.433(3)		
Bond angles			
N(2)−Fe(1)−N(3)	95.67(9)	C(12)−C(11)−C(19)	123.6(2)
N(2)−Fe(1)−Cl(1)	90.39(7)	N(2)−C(12)−C(11)	125.4(3)
N(3)−Fe(1)−Cl(1)	89.09(7)	C(18)−C(13)−N(2)	114.2(2)
C(12)−N(2)−C(13)	121.4(2)	C(13)−C(18)−N(3)#1	114.2(2)
C(19)−N(3)−C(18)#1	121.2(2)	N(3)−C(19)−C(11)	124.9(3)

[a]Symmetry transformations used to generate equivalent atoms: #1 $-x + 1/2, -y + 3/2, -z$.

dx.doi.org/10.1021/ic302150j | Inorg. Chem. 2013, 52, 1926−1941

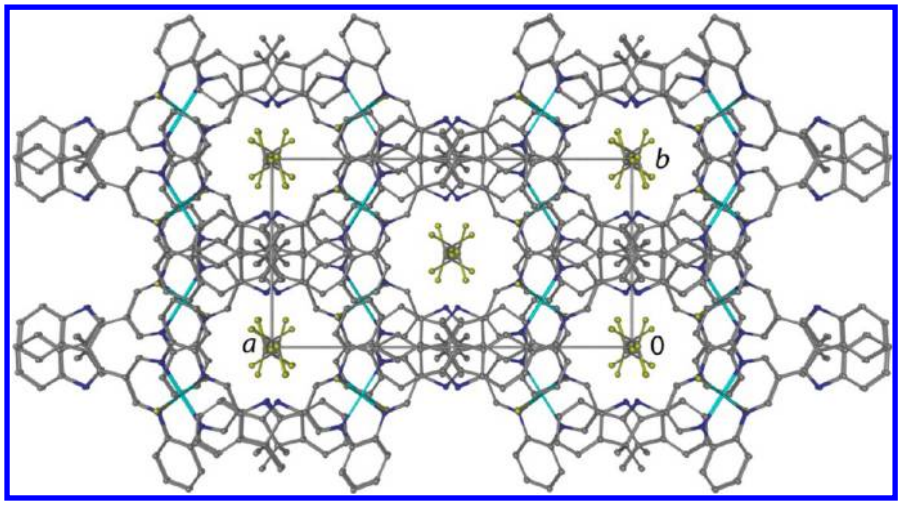

Figure 17. Crystal packing view of $[Fe(LH_2)Cl_2]^+ \cdot Cl^- \cdot CHCl_3$, showing channels along the *c*-axis, filled with the chloride anions and the solvent chloroform molecules.

Scheme 4. Synthesis of $[Pd_2(LH_2)_2(OAc)_4]$

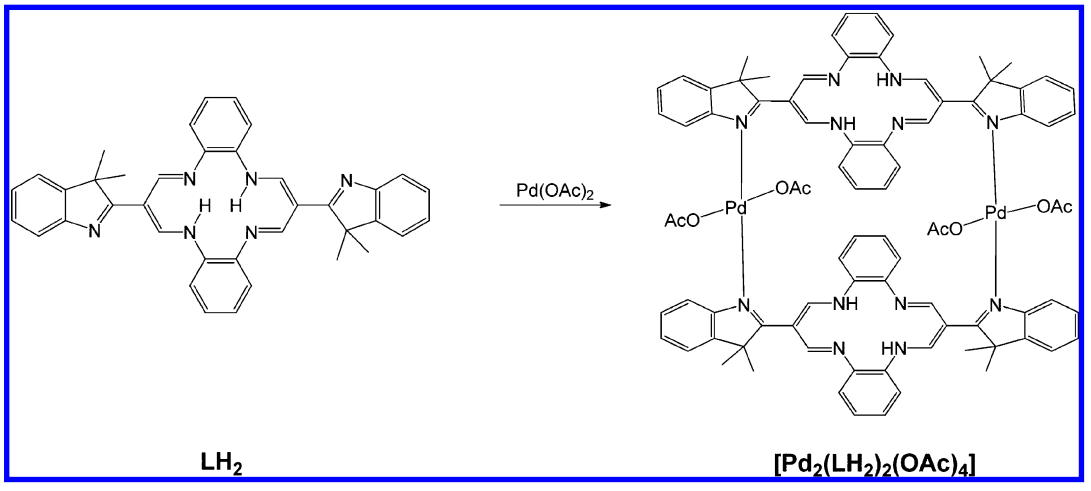

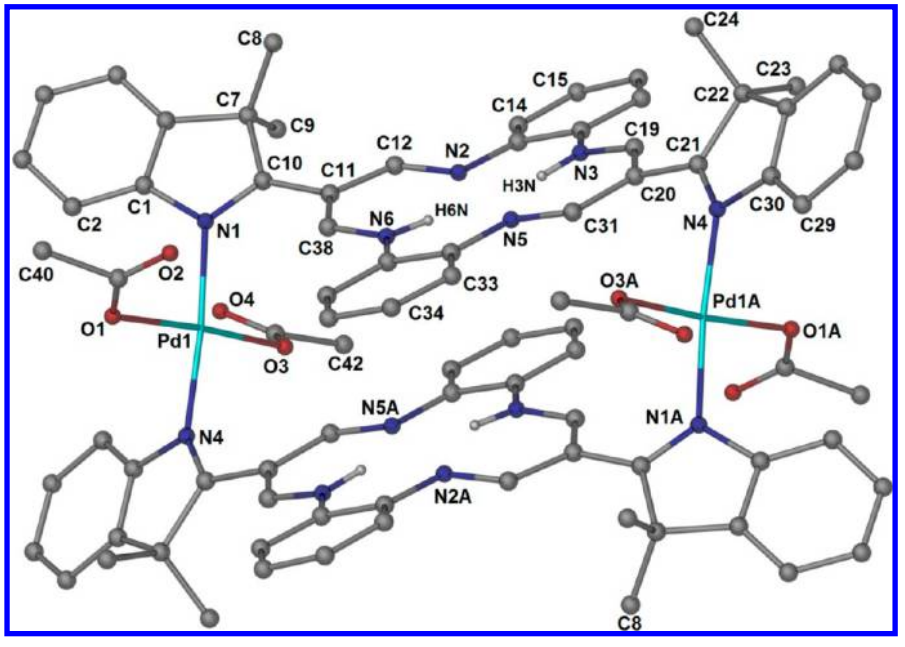

Figure 18. The molecular structure and atom labeling scheme of $[Pd_2(LH_2)_2(OAc)_4]$. C-bound hydrogen atoms are omitted for clarity.

dx.doi.org/10.1021/ic302150j | *Inorg. Chem.* 2013, 52, 1926−1941

Table 7. Selected Bond Lengths (Å) and Bond Angles (°) for $[Pd_2(LH_2)_2(OAc)_4]$[a]

Bond lengths			
Pd(1)−N(1)	2.021(5)	N(5)−C(31)	1.300(8)
Pd(1)−N(4)#1	2.020(5)	N(5)−C(32)	1.423(8)
Pd(1)−O(3)	2.030(5)	N(6)−C(38)	1.333(8)
Pd(1)−O(1)	2.053(5)	N(6)−C(37)	1.407(8)
N(1)−C(10)	1.310(8)	C(10)−C(11)	1.439(9)
N(2)−C(12)	1.295(8)	C(11)−C(38)	1.392(9)
N(2)−C(13)	1.419(8)	C(11)−C(12)	1.426(9)
N(3)−C(19)	1.328(8)	C(19)−C(20)	1.367(9)
N(3)−C(18)	1.403(8)	C(20)−C(31)	1.444(9)
N(4)−C(21)	1.301(8)	C(20)−C(21)	1.464(9)
Bond angles			
N(4)#1−Pd(1)−N(1)	172.1(2)	C(38)−C(11)−C(12)	122.4(6)
N(4)#1−Pd(1)−O(3)	90.0(2)	N(2)−C(12)−C(11)	124.8(6)
N(1)−Pd(1)−O(3)	90.2(2)	C(18)−C(13)−N(2)	116.4(6)
N(4)#1−Pd(1)−O(1)	86.2(2)	C(13)−C(18)−N(3)	116.8(6)
N(1)−Pd(1)−O(1)	93.25(19)	N(3)−C(19)−C(20)	125.3(6)
O(3)−Pd(1)−O(1)	175.6(2)	C(19)−C(20)−C(31)	122.7(6)
C(12)−N(2)−C(13)	117.7(5)	N(5)−C(31)−C(20)	123.8(6)
C(19)−N(3)−C(18)	126.5(5)	C(37)−C(32)−N(5)	117.0(5)
C(31)−N(5)−C(32)	120.4(5)	C(32)−C(37)−N(6)	118.4(5)
C(38)−N(6)−C(37)	126.5(5)	N(6)−C(38)−C(11)	123.4(6)

[a]Symmetry transformations used to generate equivalent atoms: #1 $-x + 2, -y, -z+2$.

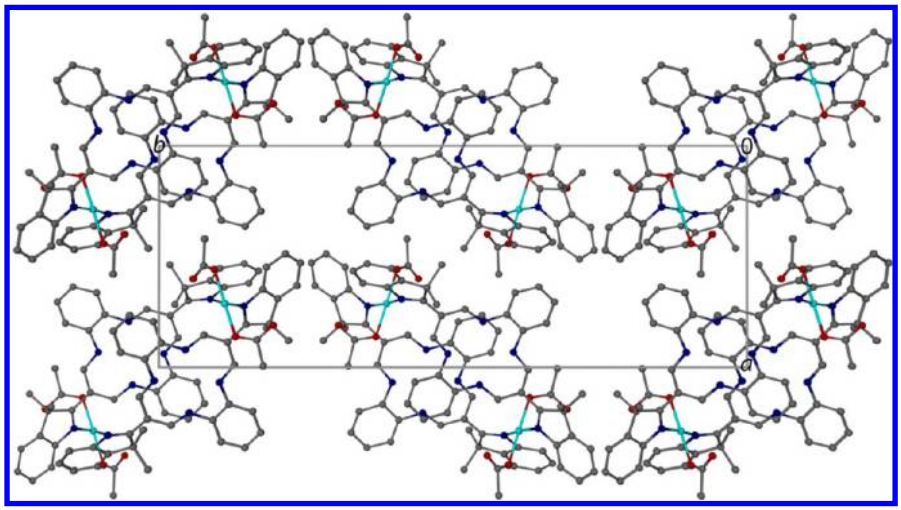

Figure 19. Crystal packing structure of $[Pd_2(LH_2)_2(OAc)_4]$, showing void spaces in the lattice.

metal coordination sites, i.e., the central cavity and the indolenine nitrogen atoms. Upon reaction with Ni^{II} or Co^{II} ions, the metal ion was inserted into the central cavity of the planar macrocycle, leading to the formation of complexes isostructural with LH_2 and thus to the alignment of the metal atoms perpendicular to the molecular plane. In [Cu(**L**)], while the metal stayed in the $[N_4]$ plane, the molecule has lost its planarity to some degree and the crystal packing shows a slipped stack arrangement, stabilized by Cu···π interactions. The Mn^{III} complexes exhibited significant displacements of the metal atoms from the $[N_4]$ plane to compensate for the longer Mn−N bond lengths. The metals are coordinated by the dianionic TAA ligand and one halogen anion in square-pyramidal geometries. In the trivalent Fe complex, the potency of the macrocyclic molecule to show imine-enamine tautomerism within the aminomethylenepropanediimine moiety allowed the ligand to remain neutral while accommodating the metal cation in the central hole. The charge balance is provided by two axially bound Cl ligands and one H-bonded chloride anion. Because of the relatively small core size of the macrocyclic ligand, Pd^{II} ion preferred to coordinate to the indolenine N donor over the $[N_4]$ donor set; thus the macrocycle behaves as a neutral ditopic ligand in $[Pd_2(LH_2)_2(OAc)_4]$ while the central core remains free.

Unless the molecules are planar and stacked perpendicular to the molecular plane (for LH_2, Ni and Co complexes) the crystal packing arrangements of the large macrocyclic molecules gave rise to frameworks that contain solvent accessible voids.

■ EXPERIMENTAL SECTION

2-(Diformylmethylidene)-3,3-dimethylindole was synthesized by a modification[38] of a procedure first described by Helliwell et al.[39] Microanalyses were carried out on a Perkin-Elmer 2400 elemental analyzer. The NMR spectra were recorded on a JEOL Lambda 400 MHz FT-NMR spectrometer. Chemical shifts are given in δ values (ppm) using TMS as the internal standard. The IR spectra were taken

dx.doi.org/10.1021/ic302150j | Inorg. Chem. 2013, 52, 1926−1941

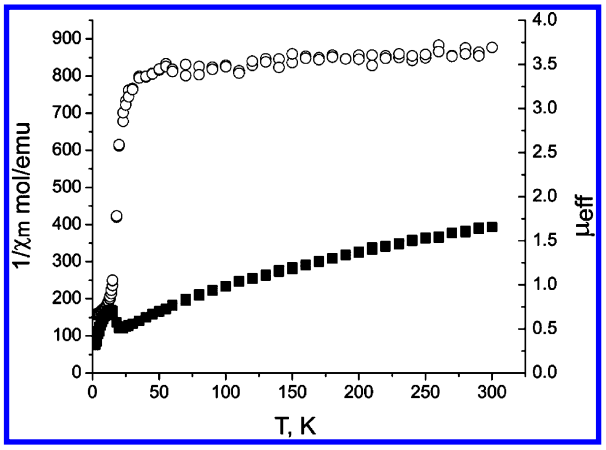

Figure 20. A plot of the magnetic behavior of the nickel complex in the temperature range 2−300 K at a field of 100 Oe. Values of $1/\chi$m are described by open circles and values of μ_{eff} are described by filled squares.

Table 8. Crystal Data and Refinement Parameters for LH_2, $LH_2{\cdot}2CHCl_3$ and $LH_4^{2+}{\cdot}2Cl^-$

	LH_2	$LH_2{\cdot}2CHCl_3$	$LH_4^{2+}{\cdot}2Cl^-$
empirical formula	$C_{38}H_{34}N_6$	$C_{40}H_{36}Cl_6N_6$	$C_{38}H_{36}Cl_2N_6$
formula weight	574.71	813.45	647.63
temperature (K)	100(2)	100(2)	90(2)
wavelength (Å)	0.71073	0.71073	0.71073
crystal system, space group	triclinic, $P\bar{1}$	monoclinic, $P2_1/n$	monoclinic, $P2_1/c$
unit cell dimensions			
a (Å)	6.8570(5)	7.9871(2)	6.6659(3)
b (Å)	14.2898(8)	19.6913(2)	14.5944(7)
c (Å)	14.9747(9)	12.3598(2)	16.4058(8)
α (°)	82.332(3)		
β (°)	85.697(4)	105.868(2)	100.606(3)
γ (°)	87.857(4)		
volume (Å^3)	1449.52(16)	1869.83(6)	1568.77(13)
Z, density (calculated) (g cm^{-3})	2, 1.317	2, 1.445	2, 1.371
F(000)	608	840	680
θ range for data collection (°)	1.38−25.05	2−27.00	2.79−27.97
reflections collected/unique	7648/4927 [R_{int} = 0.0217]	17098/4076 [R_{int} = 0.0196]	12542/3758 [R_{int} = 0.0420]
observed reflections [$I > 2\sigma(I)$]	3932	3738	2815
completeness	to θ = 25.00°: 96.2%	to θ = 27.00°: 100.0%	to θ = 27.00°: 99.4%
data/restraints/parameters	4927/2/407	4076/1/241	3758/2/216
goodness-of-fit on F^2	1.096	1.035	1.013
final R indices [$I > 2\sigma(I)$]	R_1 = 0.0778, wR_2 = 0.2138	R_1 = 0.0336, wR_2 = 0.0863	R_1 = 0.0406, wR_2 = 0.0955
R indices (all data)	R_1 = 0.0937, wR_2 = 0.2217	R_1 = 0.0366, wR_2 = 0.0885	R_1 = 0.0627, wR_2 = 0.1052
largest diff peak and hole (e Å^{-3})	0.382 and −0.331	0.517 and −0.439	0.448 and −0.398

on a Perkin-Elmer Spectrum 400 ATR-FT-IR spectrometer. The electronic spectra were measured with a Shimadzu UV-3600 UV/vis/NIR spectrophotometer in the region of 200−1100 nm. The X-ray powder diffraction was recorded on a D/Max-IIIA Bruker D8 Advance diffractometer at 40 kV, 40 mA with a Cu-target tube (λ =1.540600 Å) and a graphite monochromator. Magnetic measurements were carried

Table 9. Crystal Data and Refinement Parameters for the Ni(II), Co(II), and Cu(II) Complexes

	[Ni(**L**)]	0.73[Co(**L**)]·0.27LH_2	[Cu(**L**)]·0.5AcOH
empirical formula	$C_{38}H_{32}N_6Ni$	$C_{76}H_{65.09}Co_{1.45}N_{12}$	$C_{39}H_{34}CuN_6O$
formula weight	631.41	1231.94	666.26
temperature (K)	150(2)	100(2)	100(2)
wavelength (Å)	0.77490	0.77490	0.77490
crystal system, space group	triclinic, $P\bar{1}$	triclinic, $P\bar{1}$	orthorhombic, $P2_12_12_1$
unit cell dimensions			
a (Å)	6.896(5)	6.842(7)	5.8858(10)
b (Å)	14.223(10)	14.204(14)	15.404(3)
c (Å)	14.999(12)	14.982(15)	36.234(6)
α (°)	82.360(11)	82.306(14)	
β (°)	85.388(7)	85.505(15)	
γ (°)	87.456(7)	87.510(16)	
volume (Å^3)	1452.5(19)	1438(2)	3285.1(10)
Z, density (calculated) (g cm^{-3})	2, 1.444	1, 1423	4, 1.347
F(000)	660	644	1388
θ range for data collection (°)	3.15−27.74	3.00−25.44	4.09−33.61
reflections collected/unique	14648/5229 [R_{int} = 0.0366]	16946/4068 [R_{int} = 0.179]	43728/9960 [R_{int} = 0.0827]
observed reflections [$I > 2\sigma(I)$]	4339	2248	8551
completeness	to θ = 27.74°: 99.0%	to θ = 25.44°: 98.7%	to θ = 33.61°: 99.3%
data/restraints/parameters	5229/0/414	4068/276/416	9960/5/431
goodness-of-fit on F^2	1.028	1.075	1.049
final R indices [$I > 2\sigma(I)$]	R_1 = 0.0433, wR_2 = 0.1177	R_1 = 0.1135, wR_2 = 0.2729	R_1 = 0.0544, wR_2 = 0.1398
R indices (all data)	R_1 = 0.532, wR_2 = 0.1239	R_1 = 0.1989, wR_2 = 0.3211	R_1 = 0.0656, wR_2 = 0.1470
largest diff peak and hole (e Å^{-3})	0.649 and −0.372	1.208 and −0.872	1.063 and −0.975

out with the use of a Quantum Design MPMS SQUID magnetometer with a dc field of 100 Oe. Powdered samples were packed in a polycarbonate gel capsule. Susceptibility values were corrected for diamagnetic contributions from the gel capsule, ranging from 5.82 × 10^{-5} emu (2K) to 5.73 × 10^{-5} emu (300K) and for diamagnetism using the approximation fw/2 × 10^{-6} emu/mol.

Synthesis of LH_2, $LH_2{\cdot}2CHCl_3$ and $LH_4^{2+}{\cdot}2Cl^-$. A solution of 2-(diformylmethylidene)-3,3-dimethylindole (0.43 g, 2 mmol) and *o*-phenylene diamine (0.216 g, 2 mmol) in ethanol (40 mL) in the presence of acetic acid (0.5 mL) was refluxed for 1 h whereupon the product precipitated as an orange-red solid The solid was filtered off, washed with ethanol and dried over silica-gel, yield 0.465 g, 81%. Anal. Calc. for $C_{38}H_{34}N_6$: C, 79.41; H, 5.96; N, 14.62. Found: C, 79.00; H, 6.10; N, 14.68%. IR (ATR): ν (cm^{-1}) 3122 w, 3068 w, 2957 w, 2863 w, 1631 s, 1591 m, 1569 m, 1489 m, 1454 m, 1304 s, 1260 m, 773 m, 725 s, 530 m. ^{1}H NMR ($CDCl_3$): δ 14.58 (t, 2H, J = 6.1 Hz, N*H*); 8.95 (d, 4H, J = 6.1 Hz, C*H*N); 7.54 (d, 2H, J = 7.7 Hz, Ar-*H*); 7.40 (d, 2H, J = 6 Hz, Ar-*H*); 7.39 (d, 2H, J = 5.5 Hz, Ar-*H*); 7.33 (d, 2H, J = 7.7 Hz, Ar-*H*); 7.30 (d, 2H, J = 7.2 Hz, Ar-*H*); 7.16−7.19 (m, 6H, Ar-*H*); 1.60 (s, 12H, CH_3) ppm. ^{13}C NMR ($CDCl_3$): δ 182.44, 153.64, 150.09, 146.71, 137.56, 127.88, 126.10, 124.26, 120.77, 119.11, 115.40, 104.63, 52.56, 26.39 ppm. UV/vis (solid): λ_{max} = 536(sh), 459, 347, 275 nm.

The red crystals of LH_2, suitable for X-ray analysis, were grown from a CH_2Cl_2 solution at 5 °C. Recrystallization of the macrocyclic molecule from $CDCl_3$ gave the crystals of the chloroform solvated molecule, $LH_2{\cdot}2CHCl_3$. The crystal of the hydrochloride salt of the

dx.doi.org/10.1021/ic302150j | *Inorg. Chem.* 2013, 52, 1926−1941

Table 10. Crystal Data and Refinement Parameters for the Mn(III), Fe(III), and Pd(II) Complexes

	[Mn(**L**)Br]·0.6MeOH·0.4H_2O	[Mn(**L**)Cl]·$CHCl_3$	$[Fe(LH_2)Cl_2]^+$·Cl^-·$CHCl_3$	$[Pd_2(LH_2)_2(OAc)_4]$
empirical formula	$C_{38.60}H_{35.20}BrMnN_6O$	$C_{39}H_{33}Cl_4MnN_6$	$C_{39}H_{35}Cl_6FeN_6$	$C_{84}H_{80}N_{12}O_8Pd_2$
formula weight	733.98	782.45	856.28	1598.40
temperature (K)	100(2)	293(2)	100(2)	87(2)
wavelength (Å)	0.71073	0.71073	0.71073	1.54178
crystal system, space group	orthorhombic, $Pna2_1$	monoclinic, $P2_1/c$	monoclinic, $C2/c$	monoclinic, $P2_1/c$
unit cell dimensions				
a (Å)	31.488(6)	8.1123(11)	18.6988(17)	12.9154(3)
b (Å)	10.5599(18)	13.5986(19)	9.4611(8)	32.9705(6)
c (Å)	9.5840(16)	34.590(5)	22.402(2)	9.9792(2)
α (°)				
β (°)		103.564(3)	104.971(2)	105.367(2)
γ (°)				
volume (Å^3)	3186.8(9)	3709.4(9)	3828.7(6)	4097.49(15)
Z, density (calculated) (g cm^{-3})	4, 1.530	4, 1.401	4, 1.485	2, 1.296
F(000)	1507	1608	1756	1648
θ range for data collection (°)	2.03−29.60	1.93−27.18	2.25−25.25	3.79−56.92
reflections collected/unique	32536/8871 [R_{int} = 0.0674]	21272/8180 [R_{int} = 0.0445]	9238/3454 [R_{int} = 0.0303]	37260/5491 [R_{int} = 0.0469]
observed reflections [$I > 2\sigma(I)$]	7197	5169	2818	5086
completeness	to θ = 29.60°: 99.6%	to θ = 27.18°: 99.0%	to θ = 25.25°: 99.3%	to θ = 56.92°: 99.8%
data/restraints/parameters	8871/5/457	8180/12/483	3454/7/260	5491/2/490
goodness-of-fit on F^2	1.019	1.020	1.025	1.272
final R indices [$I > 2\sigma(I)$]	R_1 = 0.0395, wR_2 = 0.0727	R_1 = 0.0581, wR_2 = 0.1273	R_1 = 0.0422, wR_2 = 0.1101	R_1 = 0.0609, wR_2 = 0.1397
R indices (all data)	R_1 = 0.0574, wR_2 = 0.0776	R_1 = 0.1040, wR_2 = 0.1457	R_1 = 0.0564, wR_2 = 0.1184	R_1 = 0.0651, wR_2 = 0.1415
largest diff. peak and hole (e Å^{-3})	0.701 and −0.514	0.355 and −0.252	0.929 and −0.495	1.680 and −1.208

macrocycle, LH_4^{2+}·$2Cl^-$, was obtained from a solution of LH_2 in a mixture of trichloroethylene and ethylacetate in a 5 mm tube. Apparently the decomposition of trichloroethylene generates HCl and accounts for the formation of this product.

Synthesis of [Ni(L)]. A solution of nickel(II) acetate tetrahydrate (0.375 g, 0.0015 mol) in a minimum amount of water was added to a solution of LH_2 (0.575 g, 0.001 mol) in hot dioxane (130 mL). One milliliter of triethylamine was added and the mixture was refluxed for 20 h. The mixture was then cooled to room temperature and the dark red precipitate was filtered off, washed with ethanol and dried at 60 °C. Yield: 76% (0.48 g). Anal. Calcd for $C_{38}H_{32}N_6Ni$: C, 72.29; H, 5.11; N, 13.31. Found: C, 72.89; H, 5.79; N, 13.80. IR (ATR): ν (cm^{-1}) 3058 w, 2955 w, 2861 w, 1634 w, 1603 s, 1580 s, 1489 s, 1454 s, 1373 m, 1343 m, 1266 m, 1217 m, 1104 m, 975 m, 724 s, 546 s, 531 m. ^{1}H NMR ($CDCl_3$): δ 8.81 (s, 4H, C*H*N); 7.54 (d, 2H, J = 6 Hz, Ar-*H*); 7.53 (d, 2H, J = 6 Hz, Ar-*H*); 7.47 (d, 2H, J = 7.6 Hz, Ar-*H*); 7.24−7.28 (m, 4H, Ar-*H*); 7.12 (t, 2H, J = 7 Hz, Ar-*H*); 7.03 (d, 2H, J = 6 Hz, Ar-*H*); 7.02 (d, 2H, J = 6 Hz, Ar-*H*); 1.56 (s, 12H, CH_3) ppm. UV/vis (solid): λ_{max} = 495, 388, 281 nm. X-ray quality crystals were obtained *via* slow evaporation of a chloroform solution of the compound in a 5 mm tube.

Synthesis of [Co(L)]. A solution of $CoCl_2$ (0.14 g, 0.0011 mol) in THF (50 mL) was added to a hot solution of LH_2 (0.575 g, 0.001 mol) in the same solvent (150 mL). A few drops of triethylamine were added and the mixture was refluxed for 3 h. After being cooled to room temperature, the brownish precipitate was filtered, washed with ethanol and dried at 60 °C to yield 86% (0.541 g) of the cobalt complex. Anal. Calcd for $C_{38}H_{32}CoN_6$: C, 72.26; H, 5.11; N, 13.31. Found: C, 72.61; H, 5.22; N, 13.27. IR (ATR): ν (cm^{-1}) 3060 w, 2956 w, 2862 w, 1633 m, 1592 m, 1575 s, 1489 s, 1454 s, 1369 m, 1341 m, 1266 m, 1217 m, 1105 m, 975 m, 725 s, 550 s, 532 m. UV/vis (solid): λ_{max} = 846, 582 (sh), 489, 349, 273 nm. Cocrystals of 0.73[Co(**L**)]. 0.27LH_2 were grown by slow diffusion of pentane into a chloroform solution of a 2:1 mixture of the cobalt(II) complex and the free ligand in a 5 mm tube.

Synthesis of [Cu(L)]. The copper(II) complex was prepared following the same procedure as for [Co(**L**)] except for using $CuCl_2$ (0.15 g, 0.0011 mol) as the metal source. Yield 84% (0.533 g). Anal. Calcd for $C_{38}H_{32}CuN_6$: C, 71.73; H, 5.07; N, 13.21. Found: C, 72.54; H, 5.38; N, 13.29. IR (ATR): ν (cm^{-1}) 3056 w, 2960 w, 2861 w, 1634 w, 1598 s, 1577 s, 1491 s, 1456 s, 1375 m, 1331 s, 1265 m, 1213 s, 1105, 972, 745 s, 542 m, 525 w. UV/vis (solid): λ_{max} = 603, 509, 367, 294, 228 nm. X-ray quality crystals of [Cu(**L**)]·0.5AcOH were obtained through slow diffusion of ethyl acetate into a solution of the compound in a 1:1 mixture of acetic acid and dichloromethane.

Synthesis of [Mn(L)Br]. A chloroform solution of LH_2 in a 5 mm tube was layered by dioxane (1 cm) and this was layered by a dilute methanolic solution of $MnBr_2$·$4H_2O$. A few brown crystals of the Mn(III) complex were collected in two weeks.

Synthesis of [Mn(L)Cl]. A chloroform solution of LH_2 in a 5 mm tube was layered by a dilute methanolic solution of $MnCl_2$·$2H_2O$. A few brown crystals of the Mn(III) complex were collected in a week.

Synthesis of $[Fe(LH_2)Cl_2]^+$·Cl^-. A chloroform solution of LH_2 in a 5 mm tube was layered by a dilute methanolic solution of $FeCl_2$·$4H_2O$. The tube was set aside at room temperature for two weeks whereupon a few X-ray quality crystals of the Fe(III) complex were obtained.

Synthesis of $[Pd_2(LH_2)_2(OAc)_4]$. LH_2, (0.575 g, 0.001 mol) was dissolved in THF (150 mL) by heating. A few drops of triethylamine was added followed by the addition of a solution of palladium(II) acetate (0.224 g, 0.001 mol) in THF. The mixture was heated at reflux for 2 h and then evaporated to half volume under reduced pressure. The palladium complex which precipitated on addition of *n*-hexane to the solution, was collected and dried over silica-gel. Yield: 53% (0.42 g). Anal. Calc. for $C_{84}H_{80}N_{12}O_8Pd_2$: C, 63.12; H, 5.04; N, 10.52. Found: C, 63.99; H, 5.56; N, 11.33%. IR (ATR): ν (cm^{-1}) 1731m, 1625s, 1593m, 1558m, 1456m, 1301s, 1261m, 769m, 752s, 726s, 528m. X-ray quality crystals were grown by slow diffusion of ethyl acetate into a chloroform solution of the compound.

X-ray Crystallography and Data Collection. Diffraction data for the crystals of the free ligands, Fe(III) and Mn(III) complexes were measured using a Bruker SMART Apex II CCD area-detector diffractometer at the University of Malaya. For the nickel, cobalt and copper complexes, the crystal were mounted in the nitrogen cold stream provided by an Oxford Cryostream low temperature apparatus on the goniometer head of a Bruker D8 diffractometer equipped with an ApexII CCD detector at the Advanced Light Source, Berkeley, CA,

dx.doi.org/10.1021/ic302150j | *Inorg. Chem.* 2013, 52, 1926−1941

beamline 11.3.1. Data were collected with the use of silicon (111) monochromated synchrotron radiation (λ = 0.77490 Å). For the palladium complex, a crystal was mounted in the nitrogen cold stream provided by a CRYO Industries CryoCool low temperature apparatus on the goniometer head of a Bruker SMART ApexII DUO equipped with an Incoatec IμS Cu source at the University of California, Davis. The orientation matrix, unit cell refinement and data reduction were all handled by the Apex2 software (SAINT integration, SADABS absorption correction).[40] The structures were solved using direct or Patterson methods in the program SHELXS-97 and were refined by the full matrix least-squares method on F^2 with SHELXL-97.[41] Drawings of the molecules were produced with XSEED.[42] Crystal data and refinement parameters are summarized in Tables 8, 9, and 10.

■ ASSOCIATED CONTENT

Ⓢ Supporting Information

A packing diagram of the copper(II) complex, tables for the hydrogen bond geometry for the crystal structures, ^{1}H NMR, ^{13}C NMR, and UV−vis spectra of selected compounds, X-ray crystallographic files in CIF format, additional crystallographic refinement details for the cobalt and copper complexes. This material is available free of charge via the Internet at http://pubs.acs.org.

■ AUTHOR INFORMATION

Corresponding Author

*E-mail, hamid.khaledi@gmail.com. Tel: +603-79674246. Fax: +603-79674193.

Notes

The authors declare no competing financial interest.

■ ACKNOWLEDGMENTS

The Advanced Light Source is supported by the Director, Office of Science, Office of Basic Energy Sciences, of the U.S. Department of Energy under Contract No. DE-AC02-05CH1123. Support from the University of Malaya (HIR Grant Number UM.C/625/1/HIR/151 and UMRG Grant Number RG066/12BIO) and the Center for Natural Products and Drug Research, CENAR, (FL011-2012) is highly appreciated.

■ REFERENCES

(1) Jäger, E. G. *Z. Anorg. Chem.* **1969**, *364*, 177.
(2) Mountford, P. *Chem. Soc. Rev.* **1998**, *27*, 105.
(3) Cotton, F. A.; Czuchajowska, J. *Polyhedron* **1990**, *9*, 2553.
(4) Goedken, V. L.; Weiss, M. C. *Inorg. Synth.* **1980**, *20*, 115.
(5) Honeybourne, C. L. *Chem. Ind.* **1975**, 350.
(6) Reichardt, C.; Scheibelein, W. Z. *Naturforsch., B: Anorg. Chem., Org. Chem.* **1978**, *33B*, 1012.
(7) Sustmann, R.; Korth, H. G.; Kobus, D.; Baute, J.; Seiffert, K. H.; Verheggen, E.; Bill, E.; Kirsch, M.; de Groot, H. *Inorg. Chem.* **2007**, *46*, 11416.
(8) Honeybourne, C. L.; Burchill, P. *Inorg. Synth.* **1978**, *18*, 45.
(9) Grolik, J.; Zwoliński, K.; Sieroń, L.; Eilmes, J. *Tetrahedron* **2011**, *67*, 2623.
(10) Risitano, F.; Grassi, G.; Foti, F. *J. Heterocycl. Chem.* **2001**, *38*, 1083.
(11) Rihs, G.; Sigg, I.; Hass, G.; Winkle, T. *Helv. Chim. Acta* **1985**, *68*, 1933.
(12) Nishiwaki, N.; Ogihara, T.; Takami, T.; Tamura, M.; Ariga, M. *J. Org. Chem.* **2004**, *69*, 8382.
(13) Yatluk, Yu. G.; Suvorov, A. L. *Chem. Heterocycl. Compd.* **1987**, *23*, 316.
(14) The Cambridge Structural Database: a quarter of a million crystal structures and rising. Allen, F. H. *Acta Crystallogr., Sect. B* **2002**, *58*, 380.
(15) Dudek, L.; Grolik, J.; Kazmierska, A.; Szneler, E.; Eilmes, A.; Stadnicka, K.; Eilmes, J. *Tetrahedron Lett.* **2011**, *52*, 3597.
(16) Jubb, J.; Larkworthy, L. F.; Povey, D. C.; Smith, G. W. *Polyhedron* **1993**, *12*, 1179.
(17) Mulyana, Y.; Lindoy, L. F.; Kepert, C. J.; McMurtrie, J.; Parkin, A.; Turner, P.; Wei, G.; Wilson, J. G. *J. Inclusion Phenom. Macrocyclic Chem.* **2011**, *71*, 455.
(18) Gompper, R.; Illek, C.; Polborn, K. *Tetrahedron Lett.* **1992**, *33*, 3989.
(19) Hunziker, M.; Loeliger, H.; Rihs, G.; Hilti, B. *Helv. Chim. Acta* **1981**, *64*, 2544.
(20) Azuma, N.; Tani, H.; Ozawa, T.; Niida, H.; Tajima, K.; Sakata, K. *J. Chem. Soc., Perkin Trans.2* **1995**, 343.
(21) Goedken, V. L.; Pluth, J. J.; Peng, S. M.; Bursten, B. *J. Am. Chem. Soc.* **1976**, *98*, 8014.
(22) Williams, D. E.; Wohlauer, G.; Rundle, R. E. *J. Am. Chem. Soc.* **1959**, *81*, 755.
(23) Li, D. X.; Xu, D. J.; Xu, Y. Z. *Acta Crystallogr., Sect. E* **2003**, *59*, m1094.
(24) Hunziker, M.; Rihs, G. *Inorg. Chim. Acta* **1985**, *102*, 39.
(25) Franco, J. U.; Hammons, J. C.; Rios, D.; Olmstead, M. M. *Inorg. Chem.* **2010**, *49*, 5120.
(26) Weiss, M. C.; Gordon, G.; Goedken, V. L. *Inorg. Chem.* **1977**, *16*, 305.
(27) Macrae, C. F.; Bruno, I. J.; Chisholm, J. A.; Edgington, P. R.; McCabe, P.; Pidcock, E.; Rodriguez-Monge, L.; Taylor, R.; van de Streek, J.; Wood, P. A. *J. Appl. Crystallogr.* **2008**, *41*, 466.
(28) Whyte, A. M.; Shuku, Y.; Nichol, G. S.; Matsushita, M. M.; Awaga, K.; Robertson, N. *J. Mater. Chem.* **2012**, *22*, 17967.
(29) Hotz, R. P.; Bereman, R. D.; Purrington, S. T.; Singh, P. *J. Coord. Chem.* **1995**, *34*, 159.
(30) Andrews, P. C.; Atwood, J. L.; Barbour, L. J.; Croucher, P. D.; Nichols, P. J.; Smith, N. O.; Skelton, B. W.; White, A. H.; Raston, C. L. *J. Chem. Soc., Dalton Trans.* **1999**, 2927.
(31) Franceschi, F.; Hesschenbrouck, J.; Solari, E.; Floriani, C.; Re, N.; Rizzoli, C.; Chiesi-Villa, A. *J. Chem. Soc., Dalton Trans.* **2000**, 593.
(32) Weiss, M. C.; Goedken, V. L. *Inorg. Chem.* **1979**, *18*, 274.
(33) Turner, P.; Gunter, M. J.; Skelton, B. W.; White, A. H. *Aust. J. Chem.* **1998**, *51*, 835.
(34) Weber, B.; Gorls, H.; Rudolph, M.; Jager, E. G. *Inorg. Chim. Acta* **2002**, *337*, 247.
(35) Weber, B.; Kapplinger, I.; Gorls, H.; Jager, E. G. *Eur. J. Inorg. Chem.* **2005**, 2794.
(36) Weiss, M. C.; Bursten, B.; Peng, S. M.; Goedken, V. L. *J. Am. Chem. Soc.* **1976**, *98*, 8021.
(37) Minsky, A.; Meyer, A. Y.; Poupko, R.; Rabinovitz, M. *J. Am. Chem. Soc.* **1983**, *105*, 2164.
(38) Khaledi, H.; Saharin, S. M.; Ali, H. M.; Robinson, W. T.; Abdulla, M. A. *Acta Crystallogr., Sect. E* **2009**, *65*, o2585.
(39) Helliwell, M.; Afgan, A.; Baradarani, M. M.; Joule, J. A. *Acta Crystallogr., Sect. E* **2006**, *62*, o737.
(40) *APEX2 and SAINT*; Bruker AXS Inc.: Madison, Wisconsin, USA, 2007.
(41) Sheldrick, G. M. *Acta Crystallogr., Sect. A* **2008**, *64*, 112.
(42) Barbour, L. J. *J. Supramol. Chem.* **2001**, *1*, 189.